Materials Technology Reports 2025, 3(2), 3805.
doi: https://doi.org/10.59400/mtr3805

Review

Basic artificial intelligence for metallurgical design of acicular ferrite in weld metal

Krishnaswamy Sampath

Independent Researcher, Santa Clara, CA 95054, USA; krishna.sampath@icloud.com

CITATION

Sampath K. Basic artificial intelligence for metallurgical design of acicular ferrite in weld metal. Materials Technology Reports. 2025; 3(2): 3805. https://doi.org/10.59400/mtr3805

ARTICLE INFO

Received: 2 July 2025
Revised: 24 August 2025
Accepted: 29 August 2025
Available online: 27 September 2025

Abstract: Demand-critical applications require high strength steel (HSS) weldments with a significant spread between yield strength (YS) and ultimate tensile strength (UTS). Predominantly acicular ferrite (AF) microstructure in weld metal (WM) of a Fe-C-Mn-Ni based system is suitable for joining HSSs for demand-critical applications. Controlling carbon content in WM below 0.10 wt-%, actual or calculated transformation-start (T_S) temperature between 630 °C and 730 °C and weld cooling rate (CR) is critical in generating a high-performance AF microstructure. The Japan Welding Engineering Society (JWES) offers an artificial neural network (ANN) template at its website which is helpful in manipulating the addition of 16 elements in WM, each within a restricted range. This manipulation allows one to lower the T_{28J}/°C Charpy V-notch (CVN) test temperature of WM below −80 °C for achieving 28 Joules impact energy. Secondly, a *New* A_{r3} equation obtained using regression analysis through Machine Learning, enables manipulation of 14 elements (except P and S) in WM (all in wt-%) and weld CR (in °C/s) in achieving a predominantly AF microstructure in WM. Dilatometric analysis of selected WMs with Ti-B-Al-N-O content and limited N content below 85 ppm (0.0085 wt-%) showed that these two supplementary approaches can achieve a nearly "balanced" Ti-B-Al-N-O micro-alloying addition in WM. The above two tools allow welding engineers to use basic Artificial Intelligence (AI) system in evaluating or recognizing welding electrodes and related WMs that ensure adequate spread between YS and UTS, and a predictive T_{28J}/°C test temperature below −80 °C for demand-critical applications.

Keywords: electrode evaluation; shielded metal arc welding; database; Ti-B-Al-N-O micro-alloy additions; acicular ferrite; JWES-ANN tool; *New* Ar3 transformation temperature

1. Introduction

Certain demand-critical applications involving high strength steel (HSS) structures in earthquake-prone locations [1], submarines and aircraft carriers that fulfill mandatory explosion bulge test requirements [2], and pipelines for cold climate applications [3] particularly in northern Canada and arctic zone of Russia, often require a significant spread between yield strength (YS) and ultimate tensile strength (UTS) of both base metals (BMs) and relevant weld metals (WMs), with an YS/UTS ratio preferably below 0.90. Such demand-critical applications can benefit from a predominantly acicular ferrite (AF) microstructure in the WM of a Fe-C-Mn-Ni based HSS weldment. AF microstructure can provide a superior combination of high tensile strength—in the 500 to 800 MPa range—with exceptional ductility and low-temperature Charpy V-notch (CVN) impact toughness.

AF microstructure in the WM of a Fe-C-Mn-Ni HSS is based on specific chemical composition, processing, in particular weld cooling rate, microstructure development, mechanical properties and fracture characteristics. Most often, a predominantly AF microstructure in a WM is known to provide a "basket-weave" microstructure. Herein, a chaotic arrangement of lenticular ferrite plates forms inside the prior austenite grains [4–6]. Most often, the primary ferrite plates nucleate intra-granularly on $MnTi_2O_4$-rich spinel structures [7–9] and/or inclusions such as Al_2O_3 with an amorphous TiO layer [8–10]. The secondary ferrite plates nucleate on pre-existing ferrite plates.

The above microstructure provides a chaotic arrangement of the morphological feature. Specifically, this morphological feature is beneficial when the carbon content in WM is below 0.10 wt-%, while improving resistance to cracking and limiting crack propagation rate thereby offering exceptional CVN impact toughness at sub-zero temperatures. This type of AF in WM is specifically relevant for pipelines in northern Canada and arctic zone of Russia. One could further maximize the content of intra-granularly nucleated AF by increasing intragranular nucleation sites with the addition over 250 ppm (> 0.025 wt-%) Oxygen in WM while maintaining or exceeding a critical weld cooling rate [11].

Besides principal alloy elements in a Fe-C-Mn-Ni system, the presence of "controlled" and/or "balanced" amounts of Ti, B, Al, N and O in Fe-C-Mn-Ni alloy system is considered critical in forming certain types of non-metallic inclusions essential to intra-granularly nucleate AF microstructures. In general, addition of N at more than 100 ppm (0.01 wt-%) in HSS WMs is considered deleterious to WM CVN impact toughness [12].

Alternatively, when N content is marginally higher than 100 ppm (0.01 wt-%), one could add Ti between 30 ppm and 400 ppm (0.003 wt-% and 0.04 wt-%) and B at about 3 ppm to 40 ppm (0.0003 wt-% to 0.004 wt-%) at a Ti/B ratio at about 10. In multi-component Fe-C-Mn-Ni systems containing B, Mo, Ti and N, one could tie up B in solid-solution by forming BN (boron nitride) and $FeMo_2B_2$ boride, thereby decreasing the hardenability effect of B [13]. One could also effectively prevent the formation of BN by alloying with Ti that preferentially binds N through the formation of titanium carbonitride Ti(C,N).

Commonly, nucleation of AF is facilitated at near-good lattice matching across the inclusion surface and the resultant AF microstructural constituent. As is well known, Al, Ti, Si and Mn are strong deoxidizers. When the Al content is typically below 160 ppm (0.016 wt-%) together with Ti, B and O additions, Al tends to form Al_2O_3 inclusions with an amorphous TiO layer [6]. Presence of B enables the formation of amorphous TiO layer on the surface of Al_2O_3 inclusions [6,10]. The B absorption in the amorphous phase has been found to enhance intra-granular nucleation of AF at about 3% lattice misfit with ferrite [6, 8, 14]. The ferrite adjacent to the inclusion with the amorphous TiO layer shows the following Baker–Nutting orientation [6,8,14] relationship:

$$\mathrm{TiO}\{100\}//\mathrm{Fe}_\alpha\{100\}$$
$$\mathrm{TiO}\langle 011\rangle//\mathrm{Fe}_\alpha\langle 011\rangle$$

In WM samples containing low (50 ppm or 0.005 wt-%) and medium (150 ppm or 0.015 wt-%) Al contents, the nucleation of AF occurred on the surface of inclusions [15]. However, occurrence of AF was observed to be scarce in WM samples containing a higher (390 ppm or 0.039 wt-%) Al content [15]. Furthermore, grain boundary ferrite might form when the Al content is extremely low, much below 50 ppm (0.005 wt-%) that could potentially raise the CVN test temperature for T_{28J}/°C during impact testing [16]. Grain boundary ferrite scarcely formed in WM samples containing medium (150 ppm or 0.015 wt-%) and high (390 ppm or 0.039 wt-%) Al contents [16]. Interestingly, grain boundary ferrite is formed at a temperature just below 660 °C, prior to the onset of intra-granularly nucleated AF at a temperature just below 630 °C [16].

When Al content in WM is high, in excess of 390 ppm (0.039 wt-%), segregation of B to the austenite grain boundary is known to occur that most often suppresses the formation of grain boundary ferrite, thereby allowing $MnTi_2O_4$-rich spinel structures to form instead, thus promoting intra-granularly nucleated AF. Spinel structures [8,10] form in areas depleted in Mn but enriched with Ti and Al besides O. Mn-depleted zones are formed around Al_2O_3 inclusions surrounded by an amorphous layer of TiO. The Mn content of WMs affect the formation of AF through the formation of Mn-depleted zones [8,10,14]. When the Mn content of the WMs is high, Mn-depleted zones [14] are likely to form. The Ti_2O_3 phase has a trigonal lattice structure similar to α-Al_2O_3, and it is considered fully compatible with $MnTiO_3$ despite a slightly distorted lattice. $MnTi_2O_4$ phase belongs to the AB_2O_4 spinel group [10], which allows an easy substitution of Ti with other trivalent cations (e.g., Al) and divalent cations (e.g., Mn).

Based on the above understanding of the intra-granularly nucleated AF, welding electrode designers can possibly aim at a Ti:B ratio at about 10:1, an Al content below 100 ppm (0.01 wt-%), a N content much lower than 100 ppm (0.01 wt-%), O content over 250 ppm (>0.025 wt-%), between 630 °C and 730 °C as a desirable target temperature range for the austenite-to-AF transformation temperature (i.e., T_S) with adequate cooling rate in Fe-C-Mn-Ni WMs. Application of the above fundamental metallurgical principle to high-strength, high-toughness WMs also requires a simultaneous reduction in carbon content below 0.10 wt-% and Yurioka's CEN [17] below 0.300 to enhance weldability.

2. Objective

The objective of this research is to perform an analysis of 8 WMs of the TiBAlN series from Glyn Evans's Shielded Metal Arc (SMA) WM database [18] with limited N content below 85 ppm (0.0085 wt-%) to enable the selection of chemical composition of a prospective WM in achieving a high-performance AF microstructure. This analysis included:

1) A set of 8 selected WMs (named O, W, X, Y, Z, T, U and V) with N content below 85 ppm (0.0085 wt-%) based on Glyn Evans's SMA WM database [18] that allowed these WMs to develop valuable metallurgical insights on the formation of predominantly AF microstructure suitable for joining HSSs.

2) An Artificial Neural Network (ANN) template [19] available at Japan Welding Engineering Society (JWES) web-site, based on Glyn Evans's SMA WM database [18], allows welding electrode designers to manipulate the addition of 16 elements—C, Si, Mn, P, S, Cu, Ni, Cr and Mo in wt-%, and Nb (Cb), V, Ti, B, Al, N and O in ppm, each within a restricted range. One could estimate and/or lower the T_{28J}/°C CVN test temperature below −80 °C for achieving 28 Joules impact energy by manipulating the elemental content within restricted ranges for each elemental addition.
3) Dilatometric analysis [20–22] of 6 (O, X, Y, Z, U and V) of selected WMs to ascertain the effect of nearly "balanced" Ti-B-Al-N-O micro-alloying addition in WM in achieving a low T_S temperature, a narrower austenite-to-acicular ferrite start-to-finish (T_S–T_F) temperature range that promoted a "cloudburst" of refined, austenite-to-AF transformation, leading to a significant spread between YS and UTS during ambient tensile testing of WMs. A narrower austenite-to-acicular ferrite start-to-finish (T_S–T_F) temperature range appears critical to enable refined, high-performance AF microstructure with exceptional CVN impact toughness in WM.

3. Understanding weld metal microstructure

In Physical metallurgy, selection of chemical composition of welding electrode and WM is critical. The Glyn Evans's Fe-C-Mn-Ni SMA WM database [18] contains details of over 900 experimental SMAW electrodes and corresponding test results on WM chemical composition, all-weld-metal tensile properties and test temperature for CVN impact testing that achieved 28 J (i.e., T_{28J}/°C) and/or 100 J (i.e., T_{100J}/°C) absorbed energy. The various individual SMA WM electrodes cited in Evans's SMA WM database mostly belonged to the "basic" type. The test weld deposits were produced by a single master welder, using standardized procedures, at Oerlikon Welding Limited, Zurich, Switzerland according to *ISO 2560- Welding Consumables—Covered Electrodes for Manual Metal Arc Welding of Non-Alloy and Fine Grain Steels—Classification*, at a heat-input of 1 kJ/mm, 200 °C interpass temperature and 20 mm plate thickness. This detailed analysis examined controlling both carbon content below 0.10 wt-% and evaluated actual austenite transformation-start (T_S) temperature for developing, identifying and/or evaluating the occurrence of high-performance AF microstructure.

Depending on welding process selection and related weld cooling rate, one could generate WM microstructural development that could achieve specific ranges for UTS, YS, %El and %RA besides CVN impact (or fracture) toughness. The measurement of SMA WM chemical composition of over 900 test samples is described in "Metallurgy of Basic Weld Metal [23]," using automatic spectrography (AES-ICP) for most elements, with additional instrumental techniques for carbon, oxygen and nitrogen.

The desired WM microstructure [24] could be either predominantly diffusional transformation products (such as AF) when the desired WM strength is above 700 MPa (100 ksi), or predominantly athermal transformation products (such as bainite and/or lath martensite) when the desired WM strength is much higher than 800 MPa (116 ksi). In

this continuum, one must realize that indiscriminate lowering of various T_S temperatures could result in violation of the common progression of transformation temperatures, wherein $A_{r3} > B_S > B_F > M_S$, and lead to adverse consequences, particularly on WM toughness when diffusional transformation products are replaced by athermal transformation products in WM microstructure. When athermal transformation products such as lath martensite at carbon content lower than 0.10 wt-% are desired in WM microstructure, one could consider suitably manipulating the differences among the calculated values of ($B_S - M_S$), ($B_{50} - M_S$), or ($B_F - M_S$) temperatures, with calculated difference in ($B_F - M_S$) temperatures lower than −50 °C [25].

Suppressing various austenite decomposition (T_S) temperatures is known to induce greater nucleation rates and further refine resultant microstructural constituents [26]. In order to suppress various T_S temperatures, the welding electrode designers could use the following two means:

1) Proper control of the major (C, Si, Mn, P, S, Cu, Ni, Cr and Mo) and minor (Nb or Cb, V, Zr, Ti, B, Al, N and O) alloying elements in chemical composition of Fe–C–Mn-Ni welding electrode and WMs; and
2) Increase weld CR between 800 and 500 °C (i.e., $\Delta t_{8/5}$) to obtain significant undercooling, depending on the selection of the fusion welding process.

Yurioka's CEN [17] is generally used to evaluate the weldability of a variety of structural and pressure vessel steels, particularly to assess the need for preheat to overcome hydrogen-induced cracking (HIC). In particular, Yurioka's CEN [17] is also used to identify WMs that overmatch the tensile strength of the weldment relative to base metal tensile strength thus ensuring a joint efficiency in excess of 100% while complying with chemical composition requirements of relevant welding electrode specifications for HSSs.

$$\text{Yurioka's CEN} = C + \{A(C) \times EMU\} \tag{1}$$

where A(C) refers to the Accommodation factor that is a function of C content, while EMU refers to an elemental multiplication unit that includes the following 9 elemental additions: Si, Mn, Cu, Ni, Cr, Mo, V, Nb (Cb) and B.

$$A(C) = 0.75 + 0.25 \tanh[20 \times (C - 0.12)] \tag{2}$$

$$EMU = \{Si/24 + Mn/6 + Cu/15 + Ni/20 + (Cr + Mo + V + Nb)/5 + 5 \times B\} \tag{3}$$

Other Carbon Equivalent formulae such as CE_{IIW} [27] and P_{cm} [28] do not include all of the above 10 elements. For example, P_{cm} [28] was developed for pipeline steels, but does not include Nb (Cb) addition.

$$CE_{IIW} = C + (Mn + Si)/6 + (Cr + Mo + V)/5 + (Ni + Cu)/15 \tag{4}$$

$$P_{cm} = C + Si/30 + (Mn + Cu + Cr)/20 + Ni/60 + Mo/15 + V/10 + (5 \times B) \tag{5}$$

Modern steelmaking practices involving HSLA-65 plate steels [29] make use of Ti,

V and Nb (Cb) in limited quantities to achieve adequate control over desirable range of microstructures and mechanical properties. In particular, one may recognize that when carbon content exceeds 0.12 wt-%, the morphology of martensite changes from laths to plates [30,31] and this morphological change in WM and weld heat affected zone (HAZ) microstructure is known to adversely affect both CVN impact (or fracture) toughness and increase sensitivity to HIC, as in the hull of the first *Seawolf* submarine built with HY-100 steel, with nominal carbon content between 0.12 wt-% and 0.20 wt-% [32].

Besides change in morphology that adversely affects sensitivity to HIC, certain "other" conditions may also simultaneously occur during and/or following fusion welding. These "other" conditions [25] include: 1) a source of dissolved H (such as lubricant contamination); 2) high residual tensile stress distribution in the weldment; 3) a temperature range that did not allow significant solid-state diffusion of atomic H from the weldment; and 4) a time delay following welding that allowed atomic H to accumulate at internal "flaws" in the weldment. In view of the above potential for sensitivity to HIC, base metal dilution in WM during fusion welding requires additional consideration, and it is preferable to limit the carbon content of HSS welding electrodes to less than 0.10 wt-%.

A high value of Yurioka's CEN [17] could further adversely affect weldability. In particular, excessive Nb (Cb) additions over 250 ppm (0.025 wt-%) in Fe-C-Mn-Ni WM could significantly raise the CVN test temperature (T_{28J}/°C) for achieving 28 Joules impact energy [25,32].

Second, welding electrode designers need to reach beyond existing knowledge on electrode development and in particular avoid the selection of "rich" and "lean" compositions within the required chemical composition range of the relevant electrode specifications. A "rich" composition refers to all or most principal alloy elements such as C, Mn, Ni, Cr, Mo, and Cu at or near the top of the welding electrode specification range. A "lean" composition refers to all or most of the above principal elements at or near the bottom of the welding electrode specification range.

Based on the lessons learned regarding the effect of "rich" electrode composition on the cracking of the hull of the first *Seawolf* submarine in June and July of 1991 [32,33], welding electrode designers must avoid the selection of "rich" compositions within the required electrode specification range that could provide an unusually higher Yurioka's CEN [17] and high-strength WM at low-energy input welding conditions. Similarly, welding electrode designers must also avoid the selection of "lean" compositions within the required electrode specification range that could provide abnormally poor strength WM at high-energy input welding conditions.

Third, instead of "trial-and-error" methods, welding electrode designers could employ Constraints Based Modeling (CBM) to stipulate a set of "mutually inclusive" boundary conditions [34]. Specifically, the various constraints or "mutually inclusive" boundary conditions refer to selection of numerical ranges for austenite-transformation temperatures such as A_{r3} (ferrite-start), B_S (bainite-start) and M_S (martensite-start) besides carbon content below 0.10 wt-% and 9 other elemental alloy content though Yurioka's CEN [17].

The above set of results emphasize that welding electrode designers must avoid

"trial-and-error" methods. Instead, the welding electrode designers could relate metallurgical fundamentals in developing high-performance welding electrodes for HSSs. Welding electrode designers need to consider the effects of three basic steps including base metal dilution, avoid rich and lean compositions particularly carbon content of various types of HSSs, and CBM, to further enable successful navigation of relevant welding electrode specifications [35–37] in either developing or ascertaining superior combination of WM yield strength and CVN impact toughness.

The CBM was proposed in early 1992 to meet or exceed U.S. Navy requirements to overcome HIC witnessed in the production of the hull of the first *Seawolf* submarine [32]. The application of CBM [34] as a computational tool eliminated conventional "trial-and-error" methods and resulted in the development of a set of advanced ER-100S and ER-120S (MIL-100S and MIL-120S equivalents) solid-wire electrodes for gas metal arc (GMA) welding. These bare solid-wire electrodes for GMA welding ensured high-performance weldments in HSSs, including both HY-100 and HSLA- 100 steels used in U.S. Navy submarine and aircraft carrier construction. Following the award of US Patent 5744782 in April 1998 (https://patentimages.storage.googleapis.com/9f/be/1d/304d8bdc9a3c95/US5744782.pdf), the actual chemical compositions of these 8 experimental bare solid wire electrodes were reported in detail.

4. JWES-ANN template

In the following analysis, the CBM [34] approach is combined with JWES-ANN template [19] available at the Japan Welding Engineering Society (JWES) web-site to manipulate the addition of 16 elements—C, Si, Mn, P, S, Cu, Ni, Cr and Mo in wt-%, and Nb (Cb), V, Ti, B, Al, N and O in ppm, each within a restricted range, to achieve high-performance AF microstructure with exceptional strength and CVN impact (fracture) toughness. The individual range for each of the 16 elemental additions are shown in **Figure 1**.

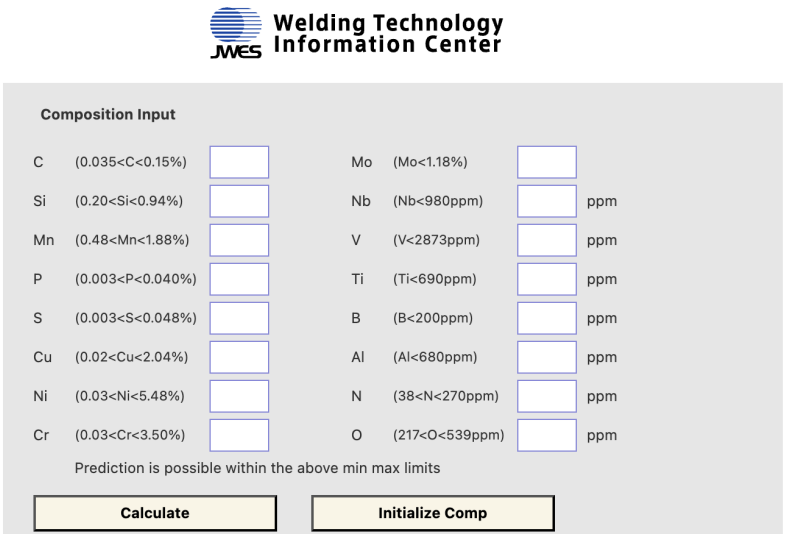

Figure 1. JWES-ANN Template with range for each elemental addition [19].

The JWES provides the above ANN template [19] at its website. Evans's SMA

WM database [18] was used in developing this ANN template with specific ranges for each of 16 elemental additions. The underlying ANN software was developed by D. J. C. MacKay at the University of Cambridge.

A key advantage of the JWES-ANN template [19] is that it allows one to manipulate the values of 16 elements (C, Si, Mn, P, S, Cu, Ni, Cr and Mo in wt-%, and Nb (Cb), V, Ti, B, Al, N, and O in ppm, as shown in **Figure 1**), with certain minimum and maximum limits for each alloy element as in JWES-ANN template of the WM chemical composition to calculate and/or predict the T_{28J}/°C CVN test temperature of Fe-C-Mn-Ni WMs that is also based on the interactive effects of chemical composition. The ANN prediction gives maximum, minimum, and average values of T_{28J}/°C along with the degree of prediction error. When the difference between the maximum and minimum predicted values is less than 30 °C, the prediction is considered reliable.

Despite the above clear advantage of the JWES-ANN template [19] in substantially reducing the risk in achieving a colder T_{28J}/°C CVN test temperature, it is well-known that using a singular value of temperature for assessing the toughness behavior of HSS weldment might potentially lead to severe limitations. While the JWES-ANN tool [19] allows one to substantially eliminate risk, the above limitation requires experimental verification to assess WM impact toughness behavior over a range of test temperatures, and to identify appropriate ductile-to-brittle transition temperature (DBTT).

Research by Bhadeshia, MacKay, and Svensson [38] describes in detail the development of an ANN technique within a Bayesian framework using CVN toughness data on SMA WM and submerged arc welded (SAW) samples. The relevant data used in this analysis were based on experimental data available at the ESAB Central Research Laboratories, Sweden. However, this ANN technique did not provide a template with certain minimum and maximum limits for each alloy element in order to estimate the CVN test temperature for achieving either T_{28J}/°C or T_{100J}/°C.

5. Shielded metal arc weld metal database

In May 2015, Dr. Evans posted online, a large, shielded metal arc (SMA) weld metal (WM) database [18]. This database contains over 900 WM compositions. Each WM composition included a listing of 16 elements—with C, Si, Mn, P, S, Cu, Ni, Cr and Mo in wt-%, and Nb (Cb), V, Ti, B, Al, N and O in ppm, as shown in **Figure 1**—along with respective WM tensile properties and CVN impact test temperatures for achieving 100 Joules (T_{100J}/°C) and 28 Joules (T_{28J}/°C) impact energy for most WM compositions. The all-WM tensile properties included YS, UTS, percent elongation (%EL) and percent reduction in area (%RA) at ambient temperature.

Evans's SMA WM database [18] is an extremely valuable resource as it provides researchers additional ability to further develop specific insights [24, 39, 40]. For example, Evans's SMA WM database [18] allowed an extensive analysis [24] of the underlying metallurgical correlations among calculated A_{r3}, B_S, B_F and M_S besides Yurioka's CEN [17] using CBM.

6. Analytical method

6.1. TiBAlN series

A part of Evans's SMA WM database [18] used an independent scheme to build a first set of 8 SMA WMs based on a TiBAlN series [41] with N content below 85 ppm (0.0085 wt-%). These 8 WMs were named O, W, X, Y, Z, T, U, and V. Weld W is considered somewhat similar to WMs deposited using Oerlikon's Tenacito 38R SMA welding electrode, currently manufactured by Lincoln Electric Company, Cleveland, OH, USA, https://www.lincolnelectric.com/en-sg/products/tenacito38r_smaw. This subset of 8 WMs focused on identification and correlation of the effects of Ti-B-Al-N-O micro-alloy additions on WM tensile properties, CVN impact toughness, and microstructure development in the fusion zone with reheated WM due to multi-pass welding.

Table 1 shows the chemical composition of 8 SMA WMs [41] belonging to the first set of TiBAlN series, with limited N content below 85 ppm (0.0085 wt-%) along with their respective Ti/B ratio, total (Ti + B + Al + N + O) content in wt-% and Yurioka's CEN [17]. The carbon content of each of these 8 WMs ranged between 0.064 wt-% and 0.078 wt-%. As mentioned earlier, when carbon content exceeds 0.12 wt-%, the morphology of martensite is likely to change from needles to plates [30, 31], and this morphological change, particularly in the weld HAZ microstructure and in reheated WM, is expected to adversely affect both CVN impact toughness and/or fracture toughness besides increasing the sensitivity to HIC.

Table 1. Chemical Composition (in wt-%) of Eight WMs with Controlled N Additions [41].

Weld ID	C	Si	Mn	P	S	Ti	B	Al	N	O	Ti/B Ratio	Ti + B + Al + N + O	Yurioka's CEN [21]
O	0.074	0.25	1.40	0.007	0.008	0.0001	0.0001	0.0006	0.0079	0.0475	1	0.0562	0.219
W	0.077	0.27	1.46	0.007	0.008	0.0028	0.0003	0.0005	0.0081	0.0459	9	0.0576	0.231
X	0.069	0.45	1.47	0.006	0.005	0.0410	0.0002	0.0001	0.0077	0.0282	205	0.0772	0.223
Y	0.070	0.45	1.57	0.010	0.006	0.0390	0.0039	0.0013	0.0083	0.0308	10	0.0833	0.244
Z	0.072	0.49	1.56	0.010	0.007	0.0420	0.0048	0.0160	0.0067	0.0438	9	0.1133	0.250
T	0.064	0.4	1.49	0.005	0.007	0.0005	0.0195	0.0005	0.0085	0.0503	0.026	0.0793	0.269
U	0.073	0.40	1.52	0.011	0.006	0.0390	0.0158	0.0005	0.0084	0.0290	2	0.0927	0.277
V	0.078	0.60	1.44	0.007	0.006	0.0540	0.0056	0.0580	0.0041	0.0440	10	0.1657	0.254
Average	0.072	0.414	1.489	0.008	0.007	0.0273	0.0063	0.0097	0.0075	0.0399	31	0.0907	0.246
High	0.078	0.6	1.57	0.011	0.008	0.0540	0.0195	0.0580	0.0085	0.0503	205	0.1657	0.277
Low	0.064	0.25	1.40	0.005	0.005	0.0001	0.0001	0.0001	0.0041	0.0282	0.026	0.0562	0.219
Range	0.014	0.35	0.17	0.006	0.003	0.0539	0.0194	0.0579	0.0044	0.0221	205	0.1095	0.058

Note: Six of other sixteen alloy additions were kept constant: Cu at 0.03 wt-%, Ni at 0.03 wt-%, Cr at 0.03 wt-%, Mo at 0.005 wt-%, Nb at 5 ppm (0.0005 wt-%) and V at 5 ppm (0.0005 wt-%).

The Si content of these 8 WMs varied between 0.25 wt-% and 0.6 wt-% and Mn content varied between 1.40 wt-% and 1.57 wt-%. Other principal alloy elements remained constant: Cu content at 0.03 wt-%, Ni content at 0.03 wt-%, Cr content at 0.03 wt-%, Mo content at 0.005 wt-%, Nb content at 5 ppm (0.0005 wt-%) and V content at 5 ppm (0.0005 wt-%). Yurioka's CEN [17] of these 8 WMs, as shown in **Table 1**, ranged from a low of 0.219 for weld O to a high of 0.277 for weld U.

Of the 8 SMA WMs belonging to the TiBAlN series [41] with N content below 85 ppm (0.0085 wt-%), the Ti content varied between 1 ppm (0.0001 wt-%) and 540 ppm (0.0540 wt-%), B content ranged between 1 ppm (0.0001 wt-%) and 195 ppm (0.0195 wt-%), Al content varied between 1 ppm (0.0001 wt-%) and 580 ppm (0.0580 wt-%), N content varied between 41 ppm (0.0041 wt-%) and 85 ppm (0.0085 wt-%) and O content varied between 282 ppm (0.0282 wt-%) and 503 ppm (0.0503 wt-%).

The combined (Ti + B + Al + N + O) content of these 8 WMs ranged from a low at 562 ppm (0.0562 wt-%) for weld O to a high at 1657 ppm (0.1657 wt-%) for weld V. Certain prior investigations involving AF microstructure in WM had revealed carbon content between 0.03 wt-% and 0.13 wt-% with N content in only two of WMs at 109 ppm ad 119 ppm [42], and carbon content between 0.034 wt-% and 0.048 wt-% while the Mn content was held between 0.36 wt-% and 1.68 wt-% [43].

As shown in **Table 1**, the Ti/B ratio of these 8 WMs ranged between 0.026 for weld T and 205 for weld X. Coincidentally, welds Y and V showed a Ti:B ratio at 10:1, while weld W showed a Ti:B ratio at 9:1.

As shown in **Table 1**, weld O contained minimal amount of Ti at 1 ppm (0.0001 wt-%), B at 1 ppm (0.0001 wt-%) and Al at 6 ppm (0.0006 wt-%) but excessive amount of O at 475 ppm (0.0475 wt-%). Similarly, weld T contained minimal amount of Ti at 5 ppm (0.0005 wt-%) but excessive amounts of both B at 195 ppm (0.0195 wt-%) and O at 503 ppm (0.0503 wt-%) than weld X that contained excessive amount of Ti at 410 ppm (0.0410 wt-%) but B at 2 ppm (0.0002 wt-%) and O at 282 ppm (0.0282 wt-%). Weld T likely had more free oxygen in solution than perhaps weld U that contained excessive amount of Ti at 390 ppm (0.0390 wt-%) but B at 158 ppm (0.0158 wt-%) and O at 290 ppm (0.0290 wt-%).

6.2. Weld mechanical properties

Weld mechanical testing of these 8 WMs, with a predominantly AF microstructure, included all-WM tensile properties and CVN impact testing over a broad temperature range from −120 °C to +40 °C [41]. **Table 2** shows the experimental results on ambient temperature tensile testing. The ambient temperature tensile test results revealed that weld V showed the highest YS at 668 MPa and UTS at 732 MPa. In contrast, weld O revealed the lowest YS at 445 MPa and lowest UTS at 528 MPa consistent with its lowest Yurioka's CEN [17] at 0.219. Coincidentally, weld O showed the highest tensile elongation at 28.2% while weld V showed the lowest tensile elongation at 20.3%.

Interestingly, as shown in **Table 1**, weld X with a total (Ti + B + Al + N + O) content at 772 ppm (0.0772 wt-%) showed the highest tensile reduction in area at 79.8%. In contrast, weld V with the highest total (Ti + B + Al + N + O) content at 1657 ppm (0.1657 wt-%) showed the lowest tensile reduction in area at 69.7%. Weld Z showed the highest YS/UTS ratio at 0.95, but weld O showed the lowest YS/UTS ratio at 0.84. Tensile test results with a low YS/UTS ratio means a higher spread between YS and UTS, thereby ensuring a higher tensile ductility and most likely excellent low-temperature CVN impact (fracture) toughness suitable for certain demand-critical applications. As mentioned earlier, these demand-critical applications often require significant spread between YS and UTS of both base metals and relevant weldments.

Table 2 also shows the experimental results on T_{100J}/°C and T_{28J}/°C CVN test temperatures for all 8 WMs. The T_{100J}/°C and T_{28J}/°C refer to test temperatures that achieved 100 Joules, and 28 Joules absorbed energy during CVN impact testing, respectively. Incidentally, weld Y showed both the coolest T_{100J}/°C and T_{28J}/°C test temperatures at −84 °C and −114 °C, respectively, offering exceptional low-temperature impact toughness, possibly based on Ti:B ratio at 10:1. The Ti addition

in weld Y at about 390 ppm (0.039 wt-%) and B at about 39 ppm (0.0039 wt-%) revealed a 10:1 ratio. Weld V showed the warmest T_{100J}/°C, at −12 °C even though the Ti:B ratio was held at 10. Weld O showed the warmest T_{28J}/°C, at −42 °C with a Ti:B ratio at 1. These results indicate that the selection of a Ti:B ratio could be critical [44] to weld performance during CVN impact toughness testing.

Table 2. Experimental Results on Tensile and CVN Impact Properties of 8 WMs with Controlled Ti-B-Al-N-O Additions [41].

Weld ID	WM tensile properties					CVN test temperature (°C)	
	YS (MPa)	UTS (MPa)	YS/UTS	El (%)	RA (%)	T_{100J}/°C	T_{28J}/°C
O	445	528	0.84	28.2	78.0	−14	−42
W	471	544	0.87	25.2	77	−68	−88
X	504	577	0.87	25.8	79.8	−61	−77
Y	546	594	0.92	25.8	73.0	−84	−114
Z	610	640	0.95	27.2	73.4	−83	−100
T	478	561	0.85	22.2	73.6	−34	−75
U	517	586	0.88	22.5	77.7	−53	−80
V	668	732	0.91	20.3	69.7	−12	−46
High	668	732	0.95	28.2	79.8	−12	−42
Low	445	528	0.84	20.3	69.7	−84	−114
Range	223	204	0.11	7.9	10.1	72	72

Note: Compared to welds Y and Z, the CVN test temperature (°C) for T_{100J}/°C in weld U at −53 °C appears to be related to higher B content at 158 ppm (0.0158 wt-%). Predicted T_{28J}/°C for weld U can also be improved through singular reduction in B content from 158 to 40 ppm [25] with Ti/B ratio at nearly 10:1. Welds O, X, T and V show CVN test temperature (°C) for T_{28J}/°C warmer than −80°C, perhaps due to inadequate or excessive (Ti + B + Al + N + O) content as shown in **Table 1**.

Table 3 shows the CVN impact test results in Joules over the −120 °C to +40 °C temperature range [41]. **Figure 2** shows the corresponding CVN impact toughness behavior of 8 WMs with N content less than 85 ppm (0.0085 wt-%) over the CVN test temperature range between −120 °C and +40 °C. Welds T and U showed a progressive decrease in CVN impact toughness with decreasing test temperature but without a clear indication of DBTT.

Table 3. Absorbed Energy (in Joules) of 8 WMs at CVN Test (in °C) Temperatures [41].

Weld ID	CVN test temperatures (°C)																
	−120	−110	−100	−90	−80	−70	−60	−50	−40	−30	−20	−10	0	10	20	30	40
O	2	2	2	2	3	6	9	18	30	42	64	121	158	166	174	180	186
W	3	5	10	24	56	91	122	146	162	174	184	191	196	200	202	202	202
X	3	4	5	8	22	50	107	157	176	186	196	204	212	218	219	220	221
Y	8	13	26	65	106	138	166	188	201	206	207	208	208	208	208	208	208
Z	10	14	29	65	112	146	166	178	190	202	214	226	237	240	240	240	240
T	3	6	10	16	24	34	51	70	88	107	125	141	155	169	175	179	181
U	3	4	6	10	28	51	81	110	136	154	172	188	201	208	212	214	216
V	2	2	2	2	2	5	11	23	34	48	69	109	137	146	156	160	162

Examination of the CVN impact toughness behavior showed that 5 (O, X, T, U and V) of these 8 WMs exhibited a relatively warmer CVN impact transition temperature. Both WMs Y and Z, exhibited a much lower CVN impact transition temperature. Weld W showed a marginally higher CVN impact transition temperature than welds Y and Z but a lower CVN impact transition temperature than the 5 WMs (O, X, T, U and V). As welds T, U and V had been designed to represent far extremes with either Ti, B,

Al and/or O additions despite a lower N content, their higher CVN impact transition temperature can be readily correlated with unbalanced Ti + B + Al + O content while N content was held below 85 ppm (0.0085 wt-%). The higher or warmer CVN impact transition temperature behavior of welds O, X, T, U and V can be attributed to the excessive presence of one or more Ti, B, Al and O additions.

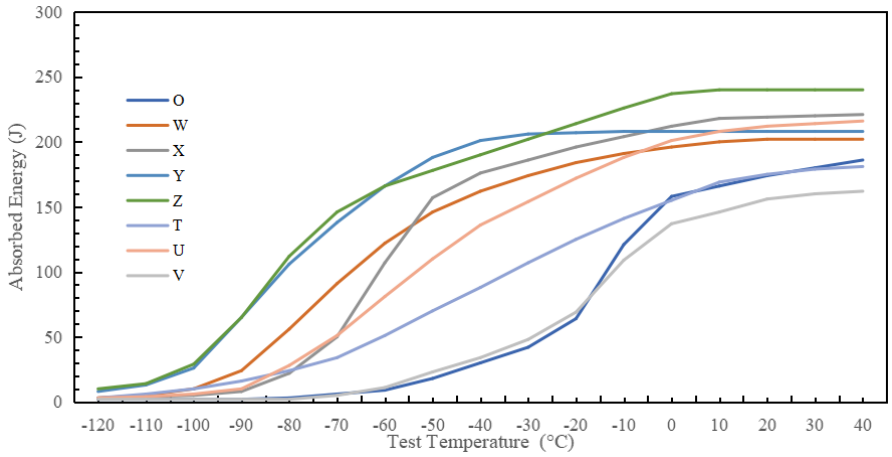

Figure 2. CVN impact toughness behavior of Ti-B-Al-N micro-alloyed WMs with N content below 85 ppm [41].

Apparently, welding electrode designers need to assess the toughness behavior of WMs with more than 100 ppm (0.001 wt-%) N and try to correlate "unbalanced" (Ti + B + Al + N + O) contents and specific aspects of WM microstructure [44]. Prior research on flux-cored arc WMs [45] had attributed a significant decrease in low-temperature impact toughness to excessive Ti and B contents that resulted in an increased volume content of upper bainite.

6.3. Two-stage selective analysis of Ti-B-Al-N-O content

A recent two-stage selective analysis [46] of Evans's SMA WM database provided additional metallurgical insight on how to lower the austenite-to-AF transformation (T_S) temperature by "balancing" Ti-B-Al-N-O microalloying additions with N content below 100 ppm (0.01 wt-%). The first-stage selective analysis considered 31 WMs in a multi-component Fe-C-Mn-Ni based compositions that substantially improved UTS, showed a significant spread between YS and UTS, with YS/UTS ratio between 0.84 and 0.95 while significantly lowering the test temperature (T_{28J}/°C) for WM CVN impact toughness at 28 Joules between −114 °C and −100 °C. The second-stage selective analysis of Evans's SMA WM database involving a cluster analysis of Ti-B-Al-N-O content in 61 WMs (**Figure 3**) revealed that "nearly" balanced (Ti + B + Al + N + O) microalloying additions could be held between 500 ppm (0.05 wt-%) and 600 ppm (0.06 wt-%) in achieving YS/UTS ratio between 0.84 and 0.92 while achieving a test temperature (T_{28J}/°C) for WM CVN impact toughness at 28 Joules between −114 °C and −90 °C.

The above selective analysis [46] further asserted that as the actual or calculated T_S temperature is lowered, one could further lower the amounts of (Ti + B + Al + N + O) micro-alloying additions in achieving further lowering of both T_S temperature

and test temperature (T_{28J}/°C) for WM CVN impact toughness at 28 Joules. A subsequent research effort [47] employed machine learning algorithm to perform regression analysis of Evans's SMA WM database [18] that was further augmented with several other related datasets. The calculated *New* A_{r3} temperature [47] of the above 61 WMs ranged between 820 °C and 646 °C temperature range, at 13 °C/s weld cooling rate.

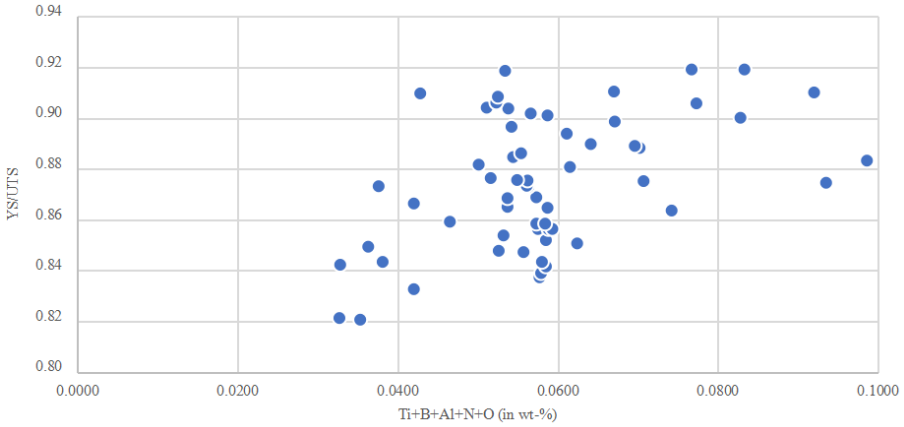

Figure 3. Clustered results show Ti-B-Al-N-O addition between 0.05 wt-% and 0.06 wt-% for achieving YS/UTS ratio between 0.84 and 0.92 [46].

7. Numerical analysis and *New* A_{r3} equation

The machine learning algorithm identified a regression equation for *New* A_{r3} equation [47] that is dependent on the presence of the following 14 elements (except P and S): C, Si, Mn, Cu, Ni, Cr, Mo, Nb (Cb), V, Ti, B, Al, N, and O (all in wt-%) and weld cooling rate (in °C/s).

$$\begin{aligned} New\ A_{r3}(^{\circ}C) = {} & 906.49 - 2.78(CR) - 439.3(C) + 34.17(Si) - 36.7(Mn) - 8.5(Cu) - 51.2(Ni) \\ & - 27.08(Cr) - 63.48(Mo) - 1765.95(Nb) - 520.29(V) - 2401.12(Ti) - 1784.44(B) \\ & + 21.89(Al) + 5300.15(N) - 420.96(O) + 297.07(C^2) - 16.4(Mn^2) \\ & + 11668.54(Nb^2) + 458.21(\sqrt{Ti}) - 1142.45(\sqrt{N}) + 298.91(\sqrt{O}) \end{aligned} \quad (6)$$

where CR refers to cooling rate in °C/s. The adjusted r^2 of this equation is relatively high at 0.9087. The intercept value of this *New* A_{r3} equation is at 906.49 °C, which is almost closer to 910 °C that corresponds to the A_{e3} (equilibrium austenite-ferrite transformation) temperature for pure iron.

The above Equation (6) shows that while addition of N in excess of 100 ppm (0.01 wt-%) is expected to increase the *New* A_{r3} temperature [47], additions of C, Nb, V, Ti and B can substantially lower the calculated values of *New* A_{r3} temperature [47], depending on weld process selection and associated weld cooling rate, requiring proper control over the above six elemental additions.

The above equation for *New* A_{r3} temperature [47] is particularly relevant for the transformation of austenite to high-performance AF microstructures in WM. **Table 4** shows the calculated *New* A_{r3} temperature (°C) of 8 WMs at 13 °C/s weld cooling rate along with the dilatometric results of 7 WMs (except weld T). Consistent with

dilatometry results, weld W showed the highest calculated *New* A_{r3} temperature at 757 °C. Interestingly, weld U showed the lowest calculated *New* A_{r3} temperature [47] at 703 °C consistent with its highest Yurioka's CEN [17] at 0.277, as shown in **Table 1**.

Table 4. Calculated and Dilatometric Results of Transformation Temperatures of WMs with Controlled Ti-B-Al-N-O Additions [20–22].

Weld ID	Calculated *New* A_{r3} temperature (°C) at 13 °C/s [47]	Dilatometric [20–22] transformation temperature (°C) at 13 °C/s		
		T_S	T_F	($T_S - T_F$)
O	750	762	554	208
W	757	764	568	196
X	736	760	568	192
Y	724	710	560	150
Z	727	710	550	160
T	722	-	-	-
U	703	700	531	169
V	728	680	507	173
High	757	764	568	208
Low	703	680	531	150
Range	54	84	37	58

Note: A comparison of the calculated *New* A_{r3} temperature [47] and T_S temperature determined using dilatometry [20–22] showed minimal difference, at about 2%, between the respective values for 5 WMs (O, W, Y, Z and U), further corroborating the utility of the *New* A_{r3} equation [47] for depressing the austenite to AF transformation temperature. Weld V showed a much larger difference between the calculated *New* A_{r3} temperature [47] and experimentally determined T_S temperature. The dilatometry results showed that weld V had a low T_S temperature at 680 °C but the (Ti + B + Al + N+ O) content was high at 0.1657 wt-% (**Table 1**). Weld V didn't show a balanced (Ti + B + Al + N+ O) content relative to their dilatometry [20–22] results.

Evidently, a comparison of the calculated *New* A_{r3} temperature [47] and experimentally determined T_S temperature showed minimal difference, at about 2%, between the respective values for 5 WMs (O, W, Y, Z and U), further corroborating the utility of the *New* A_{r3} equation for calculating austenite to AF transformation. Weld V showed a substantial difference between the calculated *New* A_{r3} temperature [47] at 728 °C while actual T_S temperature determined using dilatometry [20–22] was at 680 °C.

8. *New* A_{r3} equation and JWES-ANN tool

Table 5 shows the minimal and maximum range for elemental composition and weld CR, for both JWES-ANN template and *New* A_{r3} equation [47]. Based on **Table 5**, the minimal and maximum range for elemental composition and CR for the JWES-ANN template [19] falls within the broad range of the *New* A_{r3} equation. This basically allows the JWES-ANN template range as a valuable means for welding electrode manufacturers and welding electrode users to substantially eliminate risk in developing or ascertaining welding electrodes for specific demand-critical applications [1–3] that can benefit from a predominantly AF microstructure. Weld CR could be an additional factor depending on the choice of welding process selection such as SMA welding, spray transfer GMA welding or submerged arc welding (SAW).

Table 5. Minimum and Maximum Limits for Elemental Composition and Cooling Rate [41].

Element	JWES ANN template [19]		*New* A_{r3} equation [47]	
	Minimum (wt-%)	Maximum (wt-%)	Minimum (wt-%)	Maximum (wt-%)
C	0.035	0.15	0.024	0.792
Si	0.2	0.94	0	2.04
Mn	0.48	1.88	0	2.52
P	0.003	0.040	0	0.11
S	0.003	0.048	0	0.046
Cu	0.02	2.04	0	2.04
Ni	0.03	5.48	0	3.49
Cr	0.03	3.50	0	2.8
Mo	0	1.18	0	1.11
Nb	0	0.098	0	0.098
V	0	0.2873	0	0.099
Ti	0	0.0690	0	0.069
B	0	0.020	0	0.02
Al	0	0.0680	0	1.55
N	0.0038	0.0270	0	0.0270
O	0.0217	0.0539	0	0.118
Cooling rate (°C/s)	13		0.001	30

9. Dilatometric analysis

Dilatometric analysis [20–22] of 6 (O, X, Y, Z, U and V) of 8 SMA WMs belonging to the TiBAlN series showed the effects of specific alloy additions relative to a range of Ti, B, Al, N, and O contents, on both transformation-start (T_S) and transformation-finish (T_F) temperatures. The dilatometric evaluation [20–22] didn't include welds W and T but enabled additional metallurgical insights particularly on the effect of narrow (T_S–T_F) range in promoting a "cloudburst" of austenite-to-AF solid-state phase transformation.

The dilatometric evaluation determined the T_S (i.e., A_{r3}) and T_F temperatures during continuous cooling at 13 °C/s from 800 °C to 500 °C (i.e., $\Delta t_{8/5}$). The relevant test specimens were machined to form hollow cylinders 10 mm long × 5 mm outside diameter, with 1 mm wall thickness. The axis of the test specimen was maintained parallel to the original welding direction [20–22]. The dilatometric specimens were austenitized at 1250 °C for two minutes followed by continuous cooling at a typical SMA weld cooling rate of 13 °C/s corresponding to $\Delta t_{8/5}$.

As shown in **Table 4**, the T_S and T_F temperatures of the above 6 WMs (O, X, Y, Z, U and V) determined using dilatometry [20–22] besides a seventh weld W at a typical weld cooling rate of 13 °C/s. The T_S and T_F temperatures at 13 °C/s weld cooling rate of weld W determined using dilatometry were received through an e-mail communication from Dr. Evans. The dilatometric results revealed weld W showed the highest T_S temperature at 764 °C while weld V showed the lowest T_S temperature at 680 °C. The combined (Ti + B + Al + N + O) content of weld W at 576 ppm (0.0576 wt-%) was nearly the lowest, but marginally higher than weld O at 562 ppm (0.0562 wt-%). By contrast, the combined Ti + B + Al + N + O content of weld V at 1657 ppm (0.1657 wt-%) was the highest among all 8 WMs.

Interestingly, as shown in **Table 4**, among the 8 WMs, weld Y showed the lowest difference between T_S and T_F at 150 °C and weld O showed the highest difference between T_S and T_F temperatures at 208 °C. The 208 °C difference between T_S and T_F temperatures of weld O indicated that the total (Ti + B + Al + N + O) content at 562 ppm (0.0562 wt-%) was perhaps inadequate. Neither weld W nor weld V showed the lowest or the highest difference between T_S and T_F temperatures, perhaps due to inadequate or excessive (Ti + B + Al + N + O) content.

Surprisingly, weld Y with a 150 °C difference between T_S and T_F was followed by weld Z with a 160 °C difference. Further, weld U showed a 169 °C difference between T_S and T_F, as all three WMs contained low N content below 85 ppm (0.0085 wt-%). In weld Y, the combined (Ti + B + Al + N + O) addition at 833 ppm (0.0833 wt-%) compared to a marginally lower total (Ti + B + Al + N + O) content at 772 ppm (0.0772 wt-%) in weld X appeared to provide a balance that was perhaps nearly effective in producing a "cloudburst" of austenite-to-acicular ferrite phase transformation that likely aided the formation of refined AF microstructure over a narrow (T_S–T_F) temperature range with a corresponding YS/UTS ratio at 0.92. In weld Z, the total (Ti + B + Al + N + O) content at 1133 ppm (0.1133 wt-%) appeared somewhat excessive (over 40% compared to weld Y) that perhaps increased the difference between T_S and T_F to 160 °C while also leading to the highest YS/UTS ratio at 0.95, due to excessive (Ti + B + Al + N + O) content at 1133 ppm (0.1133 wt-%) that likely led to numerous inclusion content.

Interestingly, both weld Y (with 594 MPa UTS) and weld Z (with 640 MPa UTS) appeared closer and on either side of the trendline indicating that the (Ti + B + Al + N + O) additions are either well balanced or adequately balanced in these 2 WMs. A comparison of welds Y and Z as shown in **Tables 1, 2** and **4** revealed that at the same low, experimentally determined T_S (i.e., A_{r3}) temperature at 710 °C, one could use Ti:B at 10:1 ratio, and lesser amounts of (Ti + B + Al + N + O) content to achieve further lowering of both (T_S–T_F) temperature range and the T_{28J}/°C test temperature for achieving 28 Joules absorbed energy during CVN impact testing.

As one might expect, weld Y with combined amount of (Ti + B + Al + N + O) additions at 833 ppm (0.0833 wt-%) showed a lower YS/UTS ratio at 0.92. In weld Z, the higher combined amount of (Ti + B + Al + N + O) additions at 1133 ppm (0.1133 wt-%) appeared to contribute to a marginally higher (T_S–T_F) temperature range besides causing a higher YS/UTS ratio at 0.95. It appeared that use of lesser amount of (Ti + B + Al + N + O) reduced the (T_S–T_F) temperature range thereby promoting a "cloudburst" and "refined" austenite-to-acicular ferrite solid-state phase transformation that further lowered the YS/UTS ratio in weld Y, thereby ensuring a significant spread between YS and UTS leading to a superior combination of excellent ductility and toughness.

The comparison of welds Y and Z, both with N content below 85 ppm (0.0085 wt-%), also revealed that the balancing of Ti, B, Al and O additions maybe related to T_S, with a decreasing T_S requiring a lower amount of Ti, B, Al and O additions. For example, as shown in **Tables 1, 2** and **4**, weld V (with the highest UTS at 732 MPa of all 8 WMs together with the highest Si content at 0.6 wt-% and an excessive Al content at 580 ppm or 0.0580 wt-%) showed the lowest T_S temperature at 680 °C but a 173

°C difference between experimentally determined T_S and T_F. Even though T_S is at its lowest end at 680 °C, excessive amounts of (Ti + B + Al + N + O) additions at a total value of 1657 ppm (0.1657 wt-%) indicated the possibility to form numerous inclusions that likely produced a "dirty weld" that resulted in a higher T_{28J}/°C, at −46 °C.

By contrast, weld W showed the highest T_S temperature at 764 °C, but it contained a total (Ti + B + Al + N + O) content at 576 ppm (0.0576 wt-%). It is likely if weld W had contained higher levels of C, Mn, Cu, Ni, Cr, and Mo principal alloy additions, it would have showed a T_S (or calculated *New* A_{r3}) temperature at 690 °C or lower, and weld W might have revealed a further narrowing of the (T_S–T_F) temperature range with a total (Ti + B + Al + N + O) content at 576 ppm (0.0576 wt-%).

Furthermore, weld O with T_S at a near-high end at 762 °C, showed inadequate amount of Ti, B and Al additions likely raised T_{28J}/°C to −42 °C, indicating the possibility of free oxygen in solution. Application of JWES-ANN tool [19] showed a lowering of B content from 195 ppm to 40 ppm in weld U could help to further lower the T_{28J}/°C test temperature for 28 Joules absorbed energy from −73.6 °C to −81.3 °C during CVN impact testing, subject to experimental verification. In weld U, a higher Ti content at 390 ppm (0.039 wt-%) appears to tolerate a B content at 40 ppm (0.004 wt-%) with a Ti:B ratio nearly at 10:1, thereby predicting a lower T_{28J}/°C test temperature.

As shown in **Table 4**, the dilatometric results [20–22] on TiBAlN series of WMs with N content below 85 ppm (0.0085 wt-%) showed a "nearly" balanced (Ti + B + Al + N + O) addition in weld Y that lowered T_S temperature to 710 °C and narrowed the (T_S–T_F) temperature range to 150 °C, with actual T_{28J}/°C CVN test temperature at −114 °C. Use of controlled (not balanced) amount of (Ti + B + Al + N + O) addition in weld Y appeared to lower YS/UTS ratio to 0.92. Potentially, YS/UTS ratio lower than 0.90 could possibly indicate a "nearly" balanced (Ti + B + Al + N + O) addition that could lower the actual T_S temperature and/or narrow (T_S–T_F) temperature range, enable a high-performance WM microstructure development with exceptional mechanical properties.

The dilatometric studies [20–22] were crucial in determining the Ti-B-Al-N-O addition at 833 ppm (0.0833 wt-%) in weld Y which appeared to provide a "near" balance that was effective in producing a narrower (T_S–T_F) temperature at 150 °C, further enabling a "cloudburst" of solid-state phase transformation of austenite to AF, resulting in refined microstructural features. Due to this metallurgical effect, weld Y achieved:

1) a low T_S temperature at 710 °C due to specific WM chemical composition
2) a narrow (T_S–T_F) temperature at 150 °C due to a "nearly" balanced Ti-B-Al-N-O content at 833 ppm (0.0833 wt-%)
3) C content at 0.070 wt-%, much below 0.10 wt-%
4) Yurioka's CEN [17] at 0.244
5) actual T_{28J}/°C of −114 °C
6) actual T_{100J}/°C of −84 °C, besides
7) YS/UTS ratio at 0.92.

The YS/UTS ratio appeared marginally higher than 0.90, perhaps due to refined microstructural constituents, but one might require YS/UTS ratio lower than 0.90 for

demand-critical applications [1–3].

10. Tensile strength correlations

As illustrated in **Figure 4**, the overall trend between the experimentally determined T_S (i.e., A_{r3}) temperature and UTS among all 7 WMs (O, W, X, Y, Z, U and V except weld T) appeared highly correlated. Here the N content of all these 7 WMs was below 85 ppm (0.0085 wt-%).

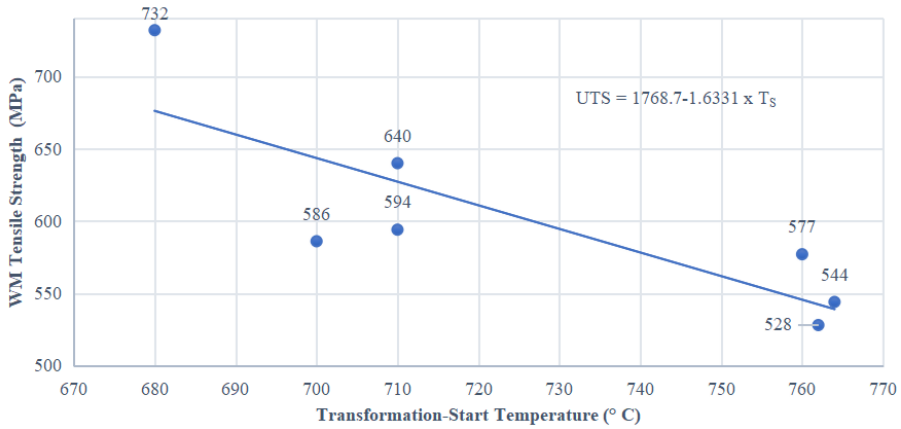

Figure 4. Effect of T_S temperature (in °C) on WM tensile strength (in MPa) with a lower N content below 85 ppm.

The trendline equation showed the following relationship between WM UTS and T_S:

$$\text{Weld metal UTS(in MPa)} = 1768.7 - (1.6331 \times T_S \text{ in °C}), \text{ with } r^2 = 0.683 \quad (7)$$

thereby clearly confirming that lowering the T_S (i.e., A_{r3}) temperature between 760 °C and 680 °C aided to increase the UTS of WMs with a predominantly AF microstructure. The trendline also confirmed the metallurgical principle that lowering the T_S temperature between 760 °C and 680 °C is essential to increase the UTS of WMs with a predominantly AF microstructure. This trendline also indicated that a T_S temperature lower than 680 °C is required to achieve a WM UTS higher than 700 MPa (100 ksi).

In general, the trendline is a useful parameter in the metallurgical design of WMs. However, scatter around the trendline is also common and the scatter is attributed to inadequate and/or excessive (Ti + B + Al + N + O) content. Bosansky and Evans [33] had attributed the scatter to a variety of additional microstructural features including variations involving types and size distributions of grains, inclusions, precipitates, etc., besides dislocation network.

Comparatively, as shown in **Table 6**, weld X with a calculated *New* A_{r3} temperature [47] at 735 °C and a marginally higher amount of Ti + B + Al + N + O addition at 772 ppm (0.0772 wt-%) showed the actual T_{28J}/°C test temperature at −77 °C during CVN impact testing. The T_{28J}/°C test temperature for 28 Joules absorbed energy during CVN impact testing could be further lowered when the actual T_S (or calculated *New* A_{r3}) temperature [47] is further lowered with appropriate levels of principal alloy

additions of C, Mn, Cu, Ni and Mo and balanced (Ti + B + Al + N + O) additions.

Table 6. Predicted CVN Test Temperature of 8 TiBAlN Series WMs with Three types of Controlled Ti-B-Al-N-O Additions [25].

Weld ID	Transformation-Start (T_S) temperature (°C) determined by dilatometry [24–26]	Calculated *New* A_{r3} temperature (°C) at 13 °C/s for original weld	YS/UTS of original weld	Experimental CVN test temperature (T_{28J}/°C)	JWES-ANN predicted CVN test temperature (T_{28J}/°C)			
					Predicted value for original weld	Predicted value when Ti-B-Al-N-O additions balanced as in weld W at 576 ppm or 0.0576 wt-%	Predicted value when Ti-B-Al-N-O additions balanced as in weld Z at 1133 ppm or 0.1133 wt-%	Predicted value when Ti-B-Al-N-O additions balanced as in weld Y at 833 ppm or 0.0833 wt-%
O	762	750	0.84	−42	−49	−82	−82	−88
W	764	760	0.87	−88	−82	-	−85	−93
X	760	735	0.87	−77	−80	−88	−90	−96
Y	710	731	0.92	−114	−102	−87	−94	-
Z	710	733	0.95	−100	−94	−88	-	−103
T	-	729	0.85	−75	−77	−87	−87	−93
U	700	708	0.88	−80	−79	−84	−92	−99
V	680	726	0.91	−46	−47	−89	−95	−103
High	764	760	0.95	−42	−47	−82	−82	−88
Low	680	708	0.84	−114	−102	−89	−95	−103

Note: While welds O, X, T and V had originally shown CVN test temperature (°C) for T_{28J}/°C warmer than −80°C, with Ti-B-Al-N-O additions as in weld W, Z or Y, the CVN test temperature (°C) for T_{28J}/°C was lowered to colder than −80°C, subject to verification.

In this context, **Table 6** clearly illustrates the benefit of "balancing" Ti, B, Al and O additions including N, as in either weld W, Z or Y. The role of JWES-ANN tool [19] in predicting this effect in substantially lowering the T_{28J}/°C test temperature for 28 Joules absorbed energy during CVN impact testing of all 8 WMs to a temperature colder than −80 °C with a predominantly AF microstructure is commendable, subject to experimental validation.

The above selective consideration of the first set of 8 WMs with low N (less than 85 ppm or 0.0085 wt-%) from the TiBAlN series indicated that "balanced" (Ti + B + Al + N + O) micro-alloying addition is expected to achieve a low T_S temperature, a narrower (T_S–T_F) temperature range, a "cloudburst" and "refined" austenite-to-AF solid-state phase transformation, a significant spread between YS and UTS during ambient tensile testing of WMs besides a predictive T_{28J}/°C test temperature lower than −80 °C for achieving 28 Joules absorbed energy during CVN impact testing.

Furthermore, **Table 7** shows the application of the *New* A_{r3} equation [47] for various WM composition with a total (Ti + B + Al + N + O) content as in welds W (576 ppm or 0.0576 wt-%), Z (1133 ppm or 0.1133 wt-%) and Y (833 ppm or 0.0833 wt-%). The total (Ti + B + Al + N + O) content as in weld W (576 ppm or 0.0576 wt-%) appears inadequate to further lower the high and low *New* A_{r3} temperatures [47] of 7 WMs. The total (Ti + B + Al + N + O) content as in weld Y (833 ppm or 0.0833 wt-%) appears to further marginally lower the *New* A_{r3} temperatures [47] of 7 WMs, and one could attribute the *New* A_{r3} temperatures [47] of 7 WMs to the Ti:B ratio at 10:1, corresponding to Ti at 390 ppm (0.039 wt-%) and B at 39 ppm (0.0039 wt-%).

Table 7. Predicted *New* A_{r3} Temperature of 8 TiBAlN Series WMs with Three types of Controlled Ti–B–Al–N–O Additions [25].

Weld ID	Transformation-start (T_S) temperature (°C) determined by dilatometry [24–26]	Calculated *New* A_{r3} temperature (°C) at 13 °C/s for original Weld	Predicted *New* A_{r3} temperature (°C) at 13 °C/s weld cooling rate		
			Predicted value when Ti-B-Al-N-O additions balanced as in weld W at 576 ppm or 0.0576 wt-%	Predicted value when Ti-B-Al-N-Oadditions balanced as in weld Z at 1133 ppm or 0.1133 wt-%	Predicted value when Ti-B-Al-N-O additions balanced as in weld Y at 833 ppm or 0.0833 wt-%
O	762	750	762	731	730
W	764	760	760	729	728
X	760	735	764	733	732
Y	710	731	763	732	731
Z	710	733	764	733	731
T	-	729	771	740	739
U	700	708	763	732	730
V	680	726	767	736	734
High	764	760	771	740	739
Low	680	708	760	729	728

Incidentally, one could also use the JWES-ANN tool [19] to identify and/or ascertain proper balancing of (Ti + B + Al + N + O) additions in predicting a T_{28J}/°C CVN absorbed energy colder than −80 °C while ensuring that the error values associated with predictions remained much lower than 30 °C. In other words, one could use a CVN test temperature colder than −80 °C as a benchmark for T_{28J}/°C to distinguish welds with nearly "balanced" (Ti + B + Al + N + O) contents.

Interestingly, as seen in **Figure 5**, the JWES-ANN tool for the average WM composition of eight WMs with a predominantly AF microstructure showed a predicted T_{28J}/°C colder than −88 °C, subject to verification. The Ti:B ratio for this average WM composition of eight WMs occurred at about 4.33.

The *New* A_{r3} temperature [47] for this average composition is predicted at 742 °C at 13 °C/s weld cooling rate using Equation (6) and the corresponding WM UTS is estimated at 557 MPa (80.8 ksi) using Equation (7). Application of the JWES-ANN tool [19] to the average WM composition shows that B content could be as high as 63 ppm (0.0063 wt-%) when the Ti content is higher at 273 ppm (0.0273 wt-%) while the Al content is seen just below 100 ppm (0.0100 wt-%). Here, the total (Ti+B+Al+N+O) content is at 907 ppm (0.0907 wt-%), consistent with a higher calculated *New* A_{r3} temperature [47] at 742 °C corresponding to 13 °C/s weld cooling rate.

As mentioned earlier, the chemical composition of weld V with the highest UTS of all 8 WMs at 732 MPa together with highest Si content at 0.60 wt-% and an excessive Al content at 580 ppm (0.0580 wt-%) showed the lowest T_S temperature at 680 °C but a 173 °C difference between T_S and T_F. Even though T_S is at its lowest end at 680 °C and despite a Ti:B ratio nearly at 10:1, the excessive amounts of Ti at 540 ppm (0.054 wt-%), B at 56 ppm (0.0056 wt-%), Al, N and O additions at a total value of 1657 ppm (0.1657 wt-%) likely formed a "dirty weld" with numerous inclusions and raised the T_{28J}/°C to −46 °C. This shows that balancing the (Ti + B + Al + N + O) content is essential to control inclusion content.

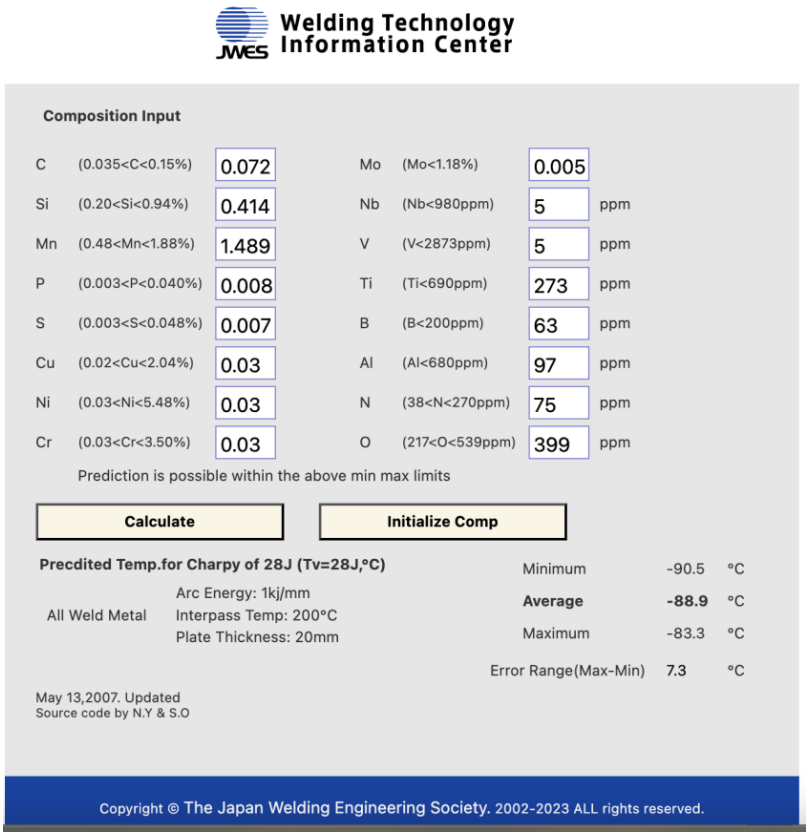

Figure 5. Effect of average composition of 8 WMs with AF microstructure on predicted T_{28J}/°C.

One could consider replacing the (Ti + B + Al + N + O) contents in weld V with a lower (Ti + B + Al + N + O) content as in weld W at 0.0576 wt-% and determine the predictive values of both T_{28J}/°C using the JWES-ANN tool [19] and the calculated *New* A_{r3} temperature [47] using Equation (6) and estimate WM UTS as well using Equation (7). As shown in **Figure 6**, the JWES-ANN tool [19] for WM composition of modified weld V (with excessive O content at 459 ppm or 0.0459 wt-%) showed a predicted T_{28J}/°C colder than −96 °C with a Ti:B ratio at nearly 10:1. The calculated *New* A_{r3} temperature [47] for this modified weld V composition is predicted at 769 °C at 13 °C/s weld cooling rate using Equation (6) and the corresponding WM UTS is estimated at 512.85 MPa (74.4 ksi) using Equation (7). With this change in (Ti + B + Al + N + O) contents, the modified weld V is likely to exhibit an YS/UTS ratio lower than 0.92 but requires experimental verification.

Figure 7 shows the application of JWES-ANN tool [19] for a typical WM composition with a total (Ti + B + Al + N + O) content at 475 ppm (0.0475 wt-%), based on a set of citations made by Ito, et al. [11], Yamada, et al. [14] and Takada, et al. [15] on O, Ti, B and Al contents. This WM composition with a Ti:B ratio at 10:1, showed a predicted T_{28J}/°C of −81.4 °C, subject to experimental verification. The calculated *New* A_{r3} temperature [47] for this typical WM composition, with a total (Ti + B + Al + N + O) content at 475 ppm (0.0475 wt-%), is predicted at 713 °C corresponding to 13 °C/s weld cooling rate using Equation (6) and the relevant WM UTS is estimated at 604 MPa (87.6 ksi) using Equation (7). The YS/UTS ratio of this typical weld requires further experimental verification.

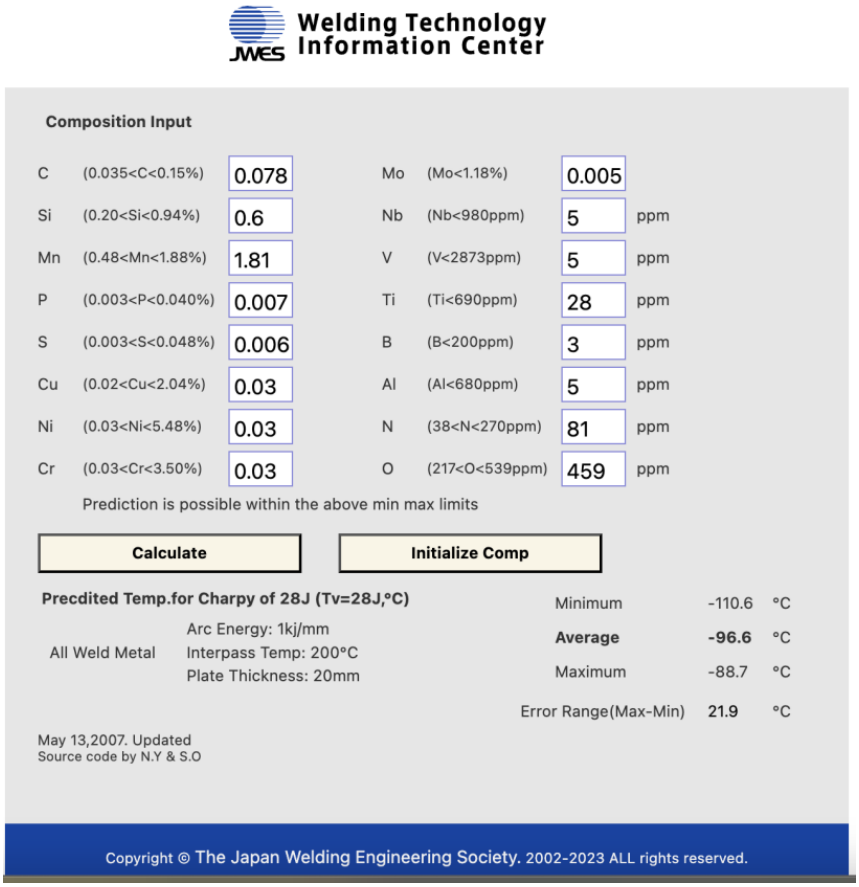

Figure 6. Effect of modified weld V composition on predicted T_{28J}/°C.

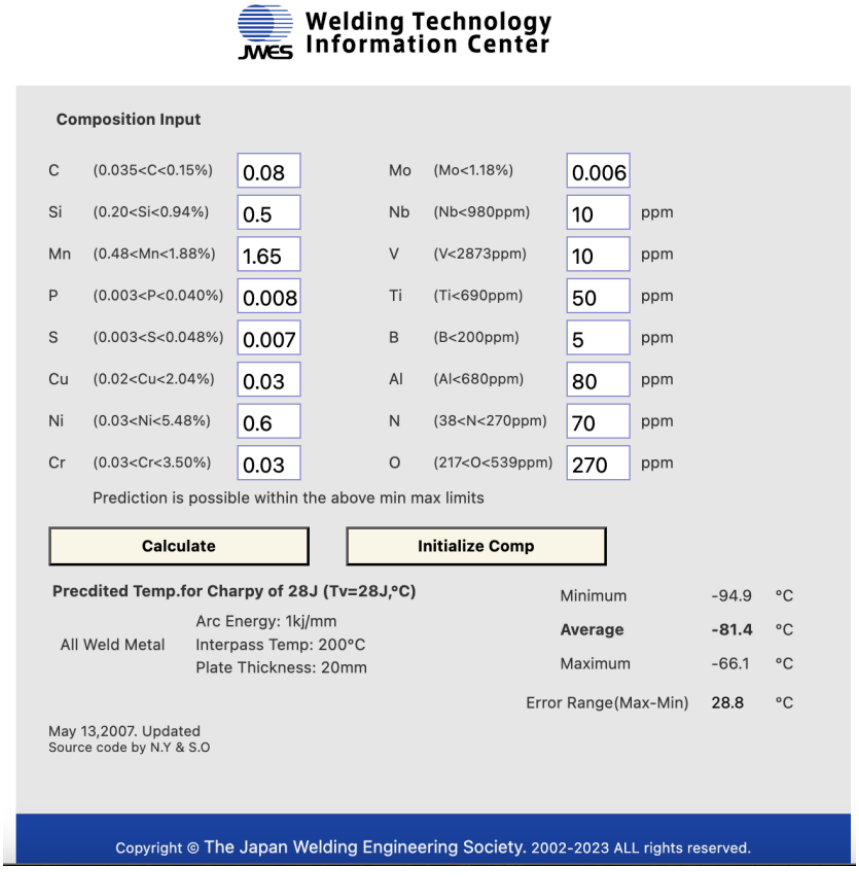

Figure 7. A typical weld metal composition with a predicted T_{28J}/°C lower than −81 °C.

11. Application of basic artificial intelligence

Furthermore, a recent research publication on "Influence of Microalloying on Precipitation Behavior and Notch Impact Toughness of Welded High-Strength Structural Steels," mentions the importance of AF in WM [48]. This research article also emphasizes mechanical properties, especially CVN impact toughness of S690QL grade (per EN 10025-6) HSLA structural steel base metal (BM), WM and HAZ, that were evaluated to understand the influence of either Nb or Ti microalloying additions on the microstructure of the HAZ and its mechanical properties. A subsequent research publication on "Effect of Ti microalloying on the local strain behavior of cross-weld tensile samples determined by digital image correlation," further reinforced prior results of G69 solid wire electrode [49].

As shown in **Table 8**, the WM chemical composition from welding electrode (G69) was low in Mn content (at 1.32 wt-%) but somewhat high in Ni content (1.43 wt-%) and had C content at 0.09 wt-%. However, these results were based on manufacturer's test report, and one is not certain what type of base metal was used in the manufacturers test report, and whether the base metal dilution caused Nb and/or Ti micro-alloy additions in WMs. Readers might wonder why the authors didn't report the actual chemical composition vis-a-vis actual mechanical properties of the WMs as they related to each of three different variations of BMs. Furthermore, the reason why the authors didn't report 3 specific types of BM with additional Nb or Ti addition, with related dilution effect and corresponding WM chemical compositions is unclear.

Table 8. Chemical Composition (in wt-%) of Tested Materials (Fe balance) Determined Using Optical Emission Spectroscopy [48].

Element	C	Si	Mn	Cr	Cu	Mo	Ni	A1	Nb	Ti	N	CET[b]	CEV[b]
BM: Stand.[a]	0.20	0.80	1.70	1.50	0.50	0.70	4.0	-	0.06	0.05	0.015	-	0.65
BM: Ref	0.09	0.30	1.61	0.18	0.02	0.30	0.19	0.10	-	-	0.0063	0.30	0.47
BM: A (Nb)	0.07	0.29	1.54	0.17	0.02	0.29	0.18	0.10	0.025	-	0.0059	0.27	0.43
BM: B (Ti)	0.07	0.30	1.53	0.17	0.02	0.30	0.19	0.10	-	0.015	0.0055	0.27	0.44
WM:G69[c]	0.09	0.43	1.32	0.2	0.09	0.55	1.43	0.002	0.001	0.019	0.007	0.33	0.56

Note: [a]EN 10025-6 S690QL; [b]EN1011-2; [c]EN ISO 16834-A-G69 6 M Mn4Ni1.5CrMo; chemical composition in accordance with the manufacturer's test report.

Table 9 listed the mechanical properties of BM and WM based on producer's test report. The YS/UTS ratio of the WM was marginally higher than 0.90. The WM CVN impact toughness is reported at 87.7 Joules at −40 °C or 64 Joules at −60 °C.

Table 9. Mechanical Properties of the Tested Materials [48].

Property	Yield strength, $R_{p0.2}$ (MPa)	Tensile strength, *Rm* (MPa)	Elongation at fracture, *A*5 (%)	Impact toughness, *Av*: −40 °C (J)	Hardness (HV)
BMs[a]	690	770 to 940	14	Min. 27	284.2 (HV1)[c]
WM:G 69[b]	733	811	21.4	87.7 (64 J at −60 °C)	264.3 (HV10)

Note: [a]EN 10025-6 S690QL, properties in accordance with the standard; [b]EN ISO16834-A-G69 6 M Mn4Ni1.5CrMo, properties from the producer's test report; [c]Hardness testing.

Table 10 shows the CVN impact toughness of three investigated WMs [48]. The

authors attribute the "relatively high impact energies of all investigated WM samples" to "the predominant AF microstructure, which is characterized by its high toughness compared to bainite." The WM fracture surfaces show variations in fibrous (F) zone, (S) shear lip zone, and (R) radial zone, each reported in % indicating Ti addition from base metal dilution in WM is marginally beneficial compared to Nb addition from base metal dilution.

Table 10. CVN impact energy of three investigated WMs.

WM	F [%]	S [%]	R [%]
Schroeder et al. [48]	24	35	41
A (Nb)	26	39	35
B (Ti)	20	40	40

One could apply the JWES-ANN template for this WM composition as well, although the JWES-ANN template had been developed only for SMA welding of 20 mm thick plates, interpass temperature at 200 °C and arc energy at 1 kJ/mm with a weld CR at 13 °C/s. Furthermore, the listing for G69 WM composition included only 11 elements (C, Si, Mn, Cr, Cu, Mo, Ni, Al, Nb, Ti and N) and didn't include P, S, V, B and O contents. A simple manipulation of P and S contents at 0.007 wt-%, Cr content at 0.03 wt-%, B content at 8 ppm (0.0008 wt-%), despite a high O content at 290 ppm (0.0290 wt-%) leads to a test temperature for 28 Joules CVN impact toughness colder than −116 °C.

Figure 8 shows the application of JWES-ANN tool [19] for a typical WM composition with a total (Ti + B + Al + N + O) content at 579 ppm (0.0579 wt-%), and further based on a set of citations made by Ito et al. on O content [11], Yamada et al. on Ti and B contents [14] and Takada et al. on Al content [15]. However, the Al content in **Figure 8** is only at 10 ppm (0.001 wt-%). Due to high Mn content at 1.32 wt-%, Ti content at 190 ppm (0.019 wt-%), B content at 19 ppm (0.0019 wt-%) and O at 290 ppm (0.029 wt-%), perhaps $MnTi_2O_4$-rich spinel structures [8, 10] aided the formation of AF. This WM composition with a Ti:B ratio at 10:1, showed a predicted T_{28J}/°C colder than −116 °C, subject to experimental verification.

Furthermore, one could also apply the *New* A_{r3} regression equation [47] that is dependent on the presence of the above 14 elements (excluding P and S). GMA welding at 1 kJ/mm energy input and preheat and interpass temperature at 100 °C with 82% Ar-18% CO_2 as shield gas mix showed a $\Delta t_{8/5}$ time (measured by laser pyrometer) at 7.8 s which indicated a weld CR at 38.46 °C/s which is often higher than 13 °C/s for SMA WMs, as reported in dilatometric studies by Ilman et al [20–22].

Application of the *New* A_{r3} equation [47] (Equation (6)) to the above WM composition as listed in the JWES-ANN template [19] revealed a T_S temperature at 587 °C. Application of Equation (7) on WM UTS (in MPa) = 1768.7 − (1.6331 × T_S in °C), with $r^2 = 0.683$ revealed a UTS of 810.07 MPa, which is marginally lower than 811 MPa UTS [48].

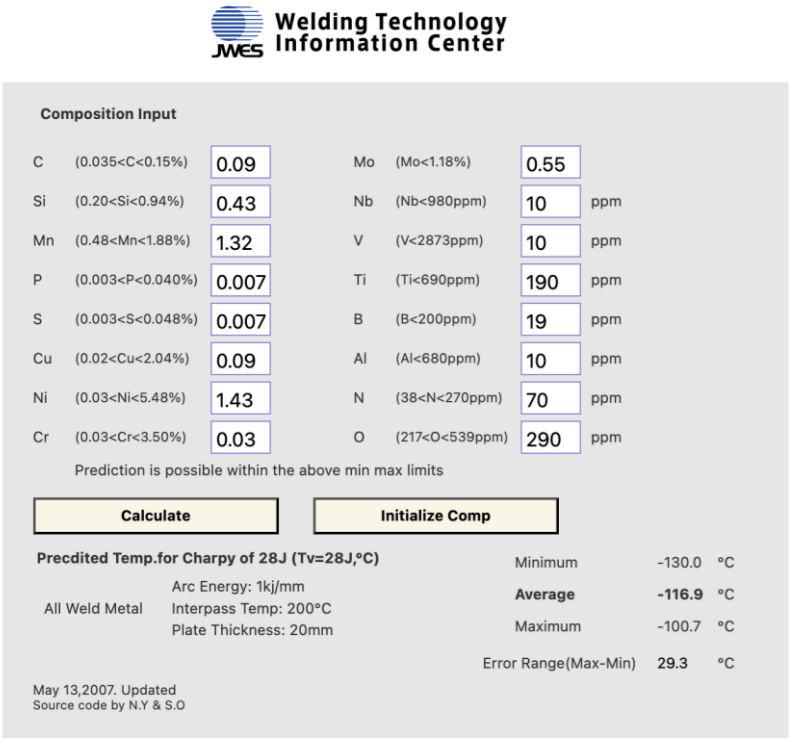

Figure 8. A typical G69 weld metal composition with a predicted T_{28J}/°C colder than −116 °C.

Based on the above examples, the Equation (6) to calculate *New* A_{r3} temperature [47] that embodies the effects of 14 major and minor alloy elements (in wt-%) besides weld CR (in °C/s) in achieving about between 630 °C and 730 °C temperature is expected to further complement the JWES-ANN template [19] for predicting T_{28J}/°C for CVN absorbed energy colder than −80 °C based on WM chemical composition. These two supplementary computational tools [19, 47] can be used with minimal risk in the efficient development and/or evaluation of welding electrode compositions based on Fe-C-Mn-Ni system that would likely provide a predominantly AF microstructure in WM to meet or exceed the requirements for high-performance and demand-critical applications.

12. Application of inverse neural network approach

A latest research publication [40] on "Inverse Neural Network Approach for Optimizing Chemical Composition in Shielded Metal Arc Weld Metals," employed a hybrid machine learning framework combining ANN with a Genetic Algorithm (GA) to optimize chemical compositions of SMA WMs based on Evans's SMA WM database for achieving targeted mechanical properties. However, the inverse neural network model, based on Bayesian optimization, didn't use austenite transformation-start (T_S) temperature. The following case settings were used for targeted WM mechanical properties, with YS at 489 MPa, UTS at 571 MPa with YS/UTS ratio at 0.86, %El at 30.2, %RA at 78, T_{28J}/°C, at −75 °C, and T_{100J}/°C, at −102 °C. Additionally, an explainable artificial intelligence (XAI) method based on Shapley values was used.

However, this inverse neural network didn't verify the predicted values. The Shapley values showed that Mn and Ni made the largest contributions to the predictions of YS, UTS, %El, %RA while N played a significant role in the predictions of T_{28J}/°C

and T_{100J}/°C. As shown in **Figure 9**, Shapley values appear to confirm the effects of both Mn content (at 1.32 wt-%) and Ni content (1.43 wt-%) of the G69 solid wire electrode used in the GMA welding of S690QL grade (per EN 10025-6) HSLA structural steel [48,49].

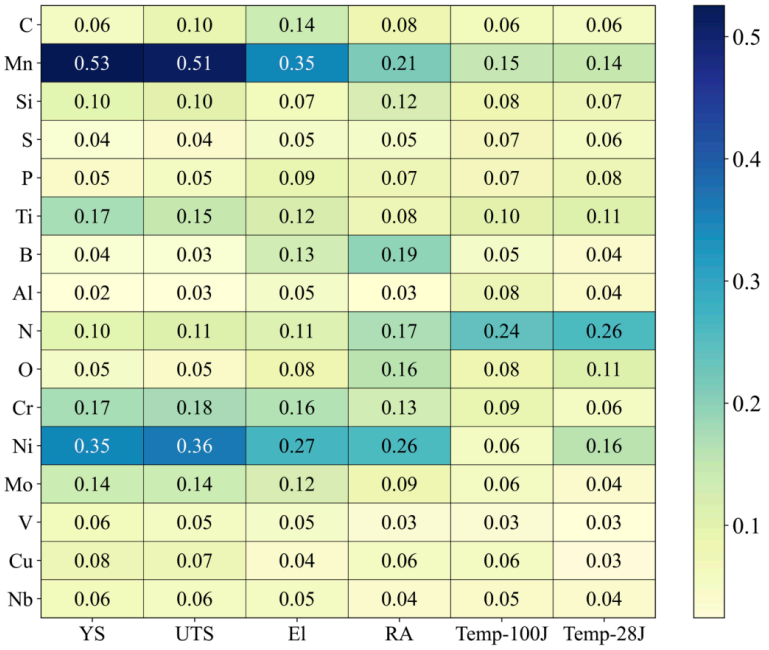

Figure 9. Shapley values of 16 elemental additions in SMA WM Database [40].

The results supposedly demonstrated high predictive accuracy for weld mechanical properties such as YS, UTS, and CVN impact transition temperatures. However, the prediction accuracy for %El and %RA appeared somewhat lower, as these properties seemed to be influenced by additional set of factors, including welding process variables, cooling rates, and microstructure formation. In fact, the authors could have used the hybrid machine learning framework combining ANN with a GA to predict UTS in excess of 640 MPa and 720 MPa, to cover a wider range as shown in **Table 2**.

The above observations suggested the need to include additional physical variables or microstructure data for future model improvements. However, the optimized WM chemical compositions generated by the GA revealed in a set of 10 trials, as shown in **Table 11**. Based on Equation (6), the tenth weld trial showed *New* A_{r3} temperature at 692 °C, at 13 °C/s weld cooling rate. Yet, excessive (Ti + B + Al + N + O) content, at or near the maximum levels for Ti, B, Al, N and O contents at 1451 ppm likely caused "dirty welds" resulting in possibly poor CVN impact toughness at T_{28J}/°C, almost similar to weld V shown in **Tables 1** and **2**.

Table 11. Optimized chemical compositions generated by the genetic algorithm [40].

Element	Trial 1	Trial 2	Trial 3	Trial 4	Trial 5	Trial 6	Trial 7	Trial 8	Trial 9	Trial 10
C (wt%)	0.035	0.038	0.038	0.035	0.035	0.041	0.038	0.037	0.039	0.035
Si (wt%)	0.731	1.081	0.823	0.437	0.926	0.036	0.016	0.648	0.019	0.033
Mn (wt%)	0.914	0.846	1.334	1.887	1.142	0.277	0.242	1.592	0.589	1.202
P (wt%)	0.003	0.006	0.003	0.008	0.003	0.003	0.003	0.003	0.009	0.003

Table 11. *Cont.*

Element	Trial 1	Trial 2	Trial 3	Trial 4	Trial 5	Trial 6	Trial 7	Trial 8	Trial 9	Trial 10
S (wt%)	0.0051	0.003	0.003	0.003	0.0073	0.003	0.003	0.008	0.003	0.0034
Cu (wt%)	0.13	0.02	0.7	0.12	0.22	0.08	0.02	0.34	0.06	0.08
Ni (wt%)	2.732	0.078	4.02	0.254	0.048	0.058	0.058	2.743	1.933	0.061
Cr (wt%)	0.061	0.065	0.245	0.262	0.091	0.104	0.062	0.036	0.104	0.266
Mo (wt%)	0.055	0.121	0.062	0.522	0.041	0.024	0.03	0.017	0.04	0.005
Nb (ppm)	7.32	539.03	12.17	7.15	19.69	3.05	630.31	62.81	5.72	43.33
V (ppm)	119.15	25.26	24.23	530.65	191.64	307.96	144.5	27.04	356	122.74
Ti (ppm)	301.44	79.08	497.91	27.84	402.34	357.53	283.78	533.76	48.53	670.27
B (ppm)	175.5	9.03	121.14	4.71	185.06	167.14	70.11	143.32	34.99	130.49
Al (ppm)	256.44	56.83	558.31	5.13	262.96	35.41	25.38	411.21	5.27	155.95
N (ppm)	120.38	111.47	136.52	152.45	152.41	195.66	44.95	227.48	126.85	249.63
O (ppm)	283.86	235.56	253.61	273.91	254.92	304	260.96	220.8	423.59	244.35

In fact, as shown in **Figure 10**, the application of JWES-ANN tool [19] showed a higher error range for CVN impact toughness at T_{28J}/°C for weld trial 10 that contained nearly contained nearly 670 ppm Ti, 130 ppm B, 156 ppm Al, 250 ppm of N and 250 ppm O, with a total Ti-B-Al-N-O content at about 1451 ppm.

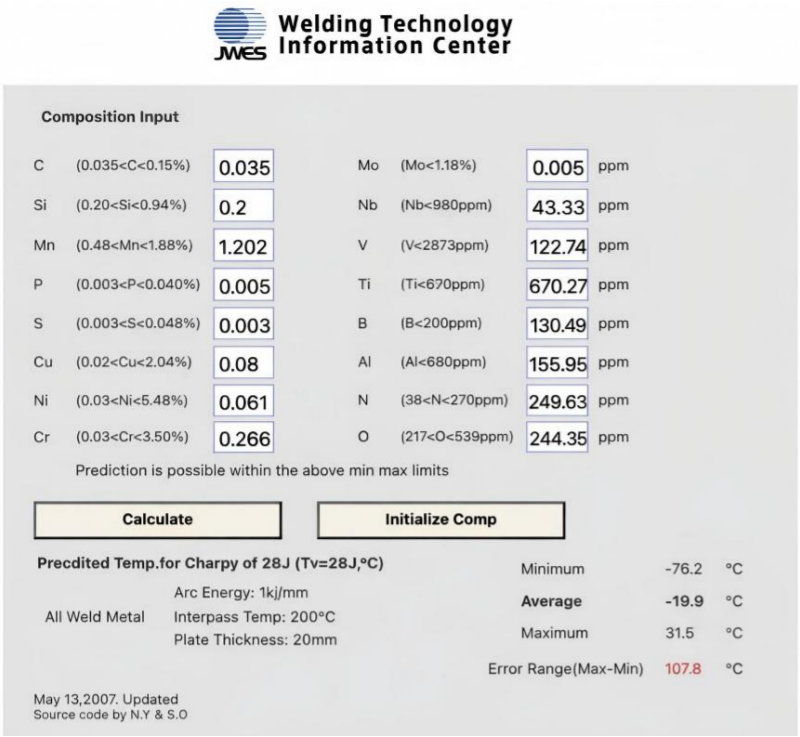

Figure 10. Trial 10 weld metal composition with a higher error range for predicted T_{28J}/°C.

13. Conclusion

Selection of consumable electrodes for fusion welding of HSSs used in the fabrication of demand-critical applications such as structures in earthquake-prone locations, aircraft carriers, submarines and pressure vessels can immensely benefit from the above understanding of the relationships among actual chemical composition, austenite-to-AF (T_S) temperature and weld CR to form predominantly AF in WM microstructures with exceptional combination of higher strength and superior CVN

impact toughness:

1) a detailed analysis of Glyn Evans's SMA WM database [18] on TiBAlN series of WMs with less than 85 ppm (0.0085 wt-%) N content affirmed that controlling carbon content much below 0.10 wt-%, CEN value below 0.300 and austenite-to-AF T_S temperature between 630 °C and 730 °C is critical in developing high-performance AF microstructures in WM;
2) achieve effective deoxidation by forming complex inclusions such as Al_2O_3 with an amorphous TiO layer, or $MnTi_2O_4$-rich spinel structures;
3) achieve a "nearly" balanced (Ti + B + Al + N + O) additions to provide a target for electrode "aim" compositions with (Ti + B + Al + N + O) content between 500 ppm (0.05 wt-%) and 600 ppm (0.06 wt-%) achieve a narrow (T_S–T_F) temperature range with a Ti:B ratio at 10:1;
4) distribute "preferred" types of inclusions to enable a "cloudburst" of a highly fracture-resistant and refined AF microstructure in WM;
5) application of JWES-ANN tool [19] could use a T_{28J} test temperature colder than −80 °C as a benchmark for achieving 28 Joules CVN impact toughness;
6) promote a significant spread between YS and UTS of WMs in ensuring excellent ductility and superior low-temperature impact toughness;
7) one could use the above two computational tools [19, 47] can be used to substantially minimize risk, eliminate "trial-and-error" methods, significantly reduce electrode development cost while meeting stringent schedule requirements;
8) these two specific computational tools could enable one to ensure efficient development and/or evaluation of welding electrode compositions based on multi-component Fe-C-Mn-Ni based system that would likely provide a predominantly AF microstructure in WM to meet or exceed the requirements for high-performance and demand-critical applications [1–3].

Funding: This work received no external funding.

Institutional review board statement: Not applicable.

Informed consent statement: Not applicable.

Data availability statement: All relevant data is provided in the article.

Conflict of interest: The author declares no conflict of interest.

References

1. American Welding Society (AWS). Structural Welding Code—Seismic Supplement. American Welding Society; 2021.
2. Schank JF, Ip C, Lacroix FW, et al. Learning from Experience, Volume II: Lessons from the U.S. Navy's Ohio, Seawolf, and Virginia Submarine Programs. RAND Corporation; 2011.
3. Ohaeri EG, Szpunar JA. An overview on pipeline steel development for cold climate applications. Journal of Pipeline Science and Engineering. 2022; 2(1): 1–17. doi: 10.1016/j.jpse.2022.01.003
4. Farrar RA, Harrison PL. Acicular ferrite in carbon-manganese weld metals: An overview. Journal of Materials Science. 1987; 22(11): 3812–3820. doi: 10.1007/BF01133327
5. Babu SS. The mechanism of acicular ferrite in weld deposits. Current Opinion in Solid State and Materials Science.

2004; 8(3–4): 267–278. doi: 10.1016/j.cossms.2004.10.001
6. Fox AG, Evans GM. A comparative study of the non-metallic inclusions in C-Mn steel weld metals containing titanium or aluminium. In: DebRoy T, David SA, DuPont JN, et al. (editors). Trends in Welding Research. ASM International; 2013. pp. 623–630.
7. Costin WL, Lavigne O, Kotousov A. A study on the relationship between microstructure and mechanical properties of acicular ferrite and upper bainite. Materials Science and Engineering: A. 2016; 663: 193–203.
8. Loder D, Michelic SK, Bernhard C. Acicular Ferrite Formation and Its Influencing Factors—A Review. Journal of Materials Science Research. 2016; 6(1): 24. doi: 10.5539/jmsr.v6n1p24
9. Kang Y, Jeong S, Kang JH, et al. Factors Affecting the Inclusion Potency for Acicular Ferrite Nucleation in High-Strength Steel Welds. Metallurgical and Materials Transactions A. 2016; 47(6): 2842–2854. doi: 10.1007/s11661-016-3456-0
10. Vezzù S, Scappin M, Boaretto D, et al. On the Effect of Slight Variations of Si, Mn, and Ti on Inclusions Properties, Microstructure, and Mechanical Properties of YS460 C-Mn Steel Welds. Metallography, Microstructure, and Analysis. 2019; 8(3): 292–306. doi: 10.1007/s13632-019-00536-1
11. Ito Y, Nakanishi M, Komizo Y. Effects of oxygen on low carbon steel weld metal. Metal Construction. 1982; 14(9): 472–478.
12. Consumables for welding of (very) high strength steels-mechanical properties of weldments in as-welded and stress-relieved applications. Available online: https://www.phase-trans.msm.cam.ac.uk/2005/LINK/90.pdf (accessed on 1 June 2025).
13. Miettinen J, Koskenniska S, Somani M, et al. Optimization of the CCT Curves for Steels Containing Al, Cu and B. Metallurgical and Materials Transactions B. 2021; 52(3): 1640–1663. doi: 10.1007/s11663-021-02130-9
14. Yamada T, Terasaki H, Komizo Y. Relation between Inclusion Surface and Acicular Ferrite in Low Carbon Low Alloy Steel Weld. ISIJ International. 2009; 49(7): 1059–1062. doi: 10.2355/isijinternational.49.1059
15. Takada A, Terasaki H, Komizo Y. Effect of aluminium content on acicular ferrite formation in low carbon steel weld metals. Science and Technology of Welding and Joining. 2013; 18(2): 91–97. doi: 10.1179/1362171812Y.0000000086
16. Takada A, Komizo YI, Terasaki H, et al. Crystallographic analysis for acicular ferrite formation in low carbon steel weld metals. Welding International. 2015; 29(4): 254–261. doi: 10.1080/09507116.2014.921042
17. Yurioka N, Suzuki H, Ohshita S, et al. Determination of necessary preheating temperature in steel welding. Welding Journal. 1983; 2(6): 147–153.
18. Evans GM. Database—Weld metal composition and properties. 2015; doi: 10.13140/RG.2.1.3628.1764
19. Charpy transition temp of all-weld-metal. Available online: https://www-it.jwes.or.jp/weld_simulator/en/cal6.jsp (accessed on 1 July 2025).
20. Ilman MN, Cochrane RC, Evans GM. Effect of Nitrogen and Boron on the Development of Acicular Ferrite iN Reheated C-Mn-Ti Steel Weld Metals. Welding in the World. 2012; 56(11–12): 41–50. doi: 10.1007/BF03321394
21. Ilman MN, Cochrane RC, Evans GM. Effect of titanium and nitrogen on the transformation characteristics of acicular ferrite in reheated C–Mn steel weld metals. Welding in the World. 2014; 58(1): 1–10. doi: 10.1007/s40194-013-0091-x
22. Ilman MN, Cochrane RC, Evans GM. The development of acicular ferrite in reheated Ti–B–Al–N-type steel weld metals containing various levels of aluminium and nitrogen. Welding in the World. 2015; 59(4): 565–575. doi: 10.1007/s40194-015-0231-6
23. Evans GM, Bailey N. Metallurgy of Basic Weld Metal. Elsevier; 1997.
24. Sampath K. Analysis of a High-Strength Steel SMAW Database. Welding Journal. 2021; 100(12): 410–420. doi: 10.29391/2022.101.036
25. Sampath K, Varadarajan R. High strength steel weld metal properties: metallurgical criteria and computational tools. Welding in the World. 2023; 67(9): 2081–2105. doi: 10.1007/s40194-023-01551-1
26. Bhadeshia HKDH. Frontiers in the Modelling of Steel Weld Deposits. Journal of The Japan Welding Society. 2007; 76(2): 102–108. doi: 10.2207/jjws.76.102
27. Dearden J, O'Neill H. A guide to the selection and welding of low alloy structural steel. Transactions of the Institute of Welding. 1940; 3: 203–214.
28. Ito Y, Bessyo K. Weldability Formula of High Strength Steels Related to Heat Affected Zone Cracking. International Institute of Welding; 1968.
29. Sampath K. An Understanding of HSLA-65 Plate Steels. Journal of Materials Engineering and Performance. 2006; 15(1): 32–40. doi: 10.1361/105994906X83439
30. Sugiyama M, Sawa G, Hata K, et al. Heterogeneous microstructure of low-carbon lath martensite with continuous

yielding behavior in Fe-C-Mn alloys. IOP Conference Series: Materials Science and Engineering. 2019; 580(1): 012045. doi: 10.1088/1757-899X/580/1/012045

31. Jorge JCF, Souza LFG, Mendes MC, et al. Microstructure characterization and its relationship with impact toughness of C–Mn and high strength low alloy steel weld metals—A review. Journal of Materials Research and Technology. 2021; 10: 471–501. doi: 10.1016/j.jmrt.2020.12.006
32. Sampath K. Three Essential Steps in Metallurgical Design of Solid Wire Electrodes for High Strength Steels. Aspects in Mining & Mineral Science. 2025; 14(1): 1694–1699.
33. Bosansky J, Evans GM. Relationships between the properties of weld metals microalloyed with V and Nb, their structure and substructure. Welding International. 1992; 6(12): 997–1002. doi: 10.1080/09507119209548332
34. Sampath K. Constraints-based modeling enables successful development of a welding electrode specification for critical navy applications. Welding Journal. 2005; 84(8): 131–138.
35. MIL-E-23765/2E, Military Specification: Electrodes and Rods—Welding, Bare, Solid, or Alloy Cored; and Fluxes, Low Alloy Steel (22 APR 1994). Available online: https://everyspec.com/MIL-SPECS/MIL-SPECS-MIL-E/MIL-E-23765-2E_12865/ (accessed on 1 July 2025).
36. American Welding Society (AWS). Specification for Low-Alloy Steel Electrodes and Rods for Gas Shielded Arc Welding. American Welding Society; 2022.
37. American Welding Society (AWS). Specification for Low-Alloy Steel Electrodes for Shielded Metal Arc Welding. American Welding Society; 2022.
38. Bhadeshia HKDH, MacKay DJC, Svensson LE. Impact toughness of C–Mn steel arc welds–Bayesian neural network analysis. Materials Science and Technology. 1995; 11(10): 1046–1051.
39. Kim JH, Jung CJ, Park YI, et al. Development of Closed-Form Equations for Estimating Mechanical Properties of Weld Metals according to Chemical Composition. Metals. 2022; 12(3): 528. doi: 10.3390/met12030528
40. Yoon T, Park YI, Kim J, et al. Inverse Neural Network Approach for Optimizing Chemical Composition in Shielded Metal Arc Weld Metals. Materials. 2025; 18(11): 2592. doi: 10.3390/ma18112592
41. Sampath K. Metallurgical Design Rules for High-Strength Steel Weld Metals. Welding Journal. 2022; 101(5): 123–143. doi: 10.29391/2022.101.010
42. Svensson LE, Gretoft DB. Microstructure and Impact Toughness of C-Mn Weld Metals. Welding Journal. 1990; 69(12): 454–461.
43. Zhang Z, Farrar RA. Influence of Mn and Ni on the Microstructure and Toughness of C-Mn-Ni Weld Metals. Welding Journal. 1997; 76(5): 184–196.
44. Johnson MQ, Evans GM, Edwards GR. The Influence of Titanium Additions and Interpass Temperature on the Microstructures and Mechanical Properties of High Strength SMA Weld Metals. ISIJ International. 1995; 35(10): 1222–1231. doi: 10.2355/isijinternational.35.1222
45. Oh DW, Olson DL, Frost RH. The influence of boron and titanium on low-carbon steel weld metal. Welding Journal. 1990; 69(4): 151–158.
46. Sampath K. Selective Analysis of a High-Strength Steel Shielded Metal Arc Weld Metal Database. Aspects in Mining & Mineral Science. 2024; 12(4). doi: 10.31031/AMMS.2024.12.000795
47. Varadarajan R, Sampath K. Application of Machine Learning to Regression Analysis of a Large SMA Weld Metal Database. Welding Journal. 2023; 102(3): 31–52. doi: 10.29391/2023.102.004
48. Schroeder N, Rhode M, Kannengiesser T. Influence of microalloying on precipitation behavior and notch impact toughness of welded high-strength structural steels. Welding in the World. 2024; 68(10): 2647–2659. doi: 10.1007/s40194-024-01827-0
49. Schroeder N, Rhode M, Kannengiesser T, et al. Effect of Ti microalloying on the local strain behavior of cross-weld tensile samples determined by digital image correlation. Welding in the World. 2025;. doi: 10.1007/s40194-025-02185-1